

Mehdi Shirani

Probabilistic and defect tolerant fatigue assessment of wind turbine castings

Thesis for the degree of Philosophiae Doctor

Trondheim, June 2011

Norwegian University of Science and Technology
Faculty of Engineering Science and Technology
Department of Engineering Design and Materials



NTNU – Trondheim
Norwegian University of
Science and Technology

NTNU

Norwegian University of Science and Technology

Thesis for the degree of Philosophiae Doctor

Faculty of Engineering Science and Technology
Department of Engineering Design and Materials

© Mehdi Shirani

ISBN 978-82-471-2850-3 (printed ver.)
ISBN 978-82-471-2851-0 (electronic ver.)
ISSN 1503-8181

Doctoral theses at NTNU, 2011:153

Printed by NTNU-trykk

Preface

This thesis consists of an introduction and seven papers [1-7]. Three papers are published and the other four ones are already submitted and are under review. The work has been carried out with supervision from Professor Gunnar Härkegård. In Paper 3 [3], the fractography and metallography were carried out by Dr Karl Martin Pedersen (Siemens Wind Power), while the analysis of the results was carried out by me. In paper 6 [6], defect size distribution was obtained by Nicolas Morin (INSA de Lyon), while other analysis was performed by me. In papers 1 to 7 [1-7], I am the main author.

Acknowledgment

This work has been made possible by the support from the Research Council of Norway and the wind turbine manufacturers Vestas Wind Systems and Siemens Wind Power through the FeVIND project. The project was carried out at the Department of Engineering Design and Materials at the Norwegian University of Science and Technology (NTNU). I would like to express my sincere gratitude to my supervisor, Professor Gunnar Härkegård who throughout my doctoral studies has contributed with excellent scientific support and encouragement, valuable ideas and suggestions and fruitful discussions. His encouragement was a major reason for me to start this work. I have learned a lot! I wish also to express my deepest gratitude to FeVIND Head Dr Morten Ingar Onsøien for always taking keen interest in my work. Furthermore, I thank my co-supervisor Dr Sigmund Kyrre Aas and also Dr Bård Wathne Tveiten, SINTEF, Trondheim. I am also grateful to excellent technical and financial support from valuable FeVIND partners Siemens Wind Power: Dr Karl Martin Pedersen, Rolf Seeberg Genz and Michael Paninski and also Vestas Wind Systems: Dr Leon Stenholt Johansen, Asger Sturlason, Bente Thomsen and Arve Krøis. Special thanks go to Dr. P. Kucharczyk and Erimar Schilberg, IEHK, RWTH, Aachen; Mr. M. Mathes, ACCESS, Aachen; Professor Stig Berge, Marintek, Trondheim; Morten Schjetne, Nomek, Trondheim and Stefan Schacht, Germanischer Lloyd Industrial Services GmbH. Finally Dr Anders Wormsen is gratefully acknowledged for enhancing and developing P•FAT.

Abstract

The present thesis deals with probabilistic and defect tolerant fatigue assessment of wind turbine castings. To this end, two types of EN-GJS-400-18-LT ductile cast iron were investigated in this research, clean baseline material in the shape of casting blocks with different thicknesses and also defective material from a rejected wind turbine hub.

To establish the required $P-S-N$ diagrams for safe-life design of wind turbine castings, fatigue specimens with different dimensions machined from baseline casting blocks with different thicknesses. Constant amplitude axial fatigue tests were performed on these specimens at room temperature at $R = 0$ and $R = -1$. Geometrical size effect, wall-thickness effect (technological size effect) and mean stress effect on fatigue strength of baseline EN-GJS-400-18-LT material were evaluated and analyzed. Statistical analysis of fatigue data was done by means of the Weibull distribution, and $P-S-N$ diagrams were established. The established $P-S-N$ diagrams showed that the Weibull distribution is well fit to the scatter of the experimentally obtained fatigue life data. Weibull's weakest-link method was used to evaluate the size effect. It made a satisfactory prediction of the fatigue strength for specimens with different dimensions.

To study damage tolerant design of wind turbine castings, a rejected wind turbine hub was flame cut to several blanks and several defective fatigue specimens were machined from these blanks. Constant amplitude axial fatigue tests were performed on these specimens at room temperature at $R = 0$ and $R = -1$. Fatigue strength of baseline EN-GJS-400-18-LT was compared with that of defective material from the rejected wind turbine hub. The effect of graphite nodules and defects type, shape, size and position on fatigue strength of defective material was evaluated. The hypothesis that the endurance observed in an $S-N$ test can be predicted based on the analysis of crack growth from casting defects through defect-free 'base' material was tested for the analyzed defective material in this research. It was shown that fatigue life of the analyzed defective cast component is controlled by fatigue crack growth and the slope of $S-N$ curve for baseline EN-GJS-400-18-LT is different than the slope of $S-N$ curve for defective EN-GJS-400-18-LT.

To perform random defect analysis of wind turbine castings, establish the scatter of fatigue life and obtain the probability of failure of these components, 3D X-ray computed tomography was used to detect defects in defective specimens and find the defect size distribution and density of defects (number of defects per unit volume). The obtained defect size distribution and density for the defective material was used in random defect analysis to establish the scatter of fatigue life for defective specimens.

Finally both safe-life and damage-tolerant design philosophies were used to evaluate the fatigue life of an EN-GJS-400-18-LT ductile cast iron block, representative of heavy-section wind turbine castings. The estimated $S-N$ curves for the analyzed component based on these two methods were compared. It was shown that fatigue design of heavy section wind turbine cast iron components based on safe-life design philosophy may result in non-conservative design of these components.

List of papers

1. M. Shirani, G. Härkegård, Fatigue life distribution and size effect in ductile cast iron for wind turbine components. *Engineering Failure Analysis* 18 (2011) 12–24.
2. M. Shirani, G. Härkegård, Large scale axial fatigue testing of ductile cast iron for heavy section wind turbine components, Submitted to *Engineering Failure Analysis*.
3. M. Shirani, K. M. Pedersen, G. Härkegård, Fatigue life prediction of heavy-section wind turbine components made of ductile cast iron containing casting defects, Submitted to *Fatigue & Fracture of Engineering Materials & Structures*.
4. M. Shirani, G. Härkegård, Fatigue crack growth simulation in components with random defects, *Journal of ASTM International* 6 (9).
5. M. Shirani, G. Härkegård, Damage tolerant design of cast components based on defects detected by 3D X-ray computed tomography, Submitted to the Special Issue 'Fatigue Design & Material Defects' of the *International Journal of Fatigue*.
6. M. Shirani, G. Härkegård, N. Morin, Fatigue life prediction of components made of spheroidal graphite cast iron, *Procedia Engineering* 2 (2010) 1125–1130.
7. M. Shirani, G. Härkegård, From safe life to damage tolerant design of wind turbine castings, Submitted to *Wind Energy*.

Contents

Preface	i
Acknowledgment	iii
Abstract	v
List of papers	vii
1 Introduction	1
1.1 Objective	1
1.2 Motivation	1
1.3 Short summary of the thesis	2
2 Safe life design	3
2.1 Experimental procedure	4
2.1.1 Material and specimens	4
2.1.1.1 T95 material	4
2.1.1.2 T150 material	4
2.2 Statistical analysis of fatigue data	5
2.2.1 Average $S - N$ curve	5
2.2.2 Linear regression to find the Basquin exponent	5
2.2.3 Weibull fatigue life distribution	5
2.2.4 $P - S - N$ diagram	5
2.3 Size effect	7
2.3.1 Geometrical size effect	7
2.3.2 Technological size effect	7
2.4 Mean stress effect	7
3 Damage tolerant design	9
3.1 Random defect analysis	12
4 Comparison of safe life design with damage tolerant design	15
5 Conclusions and suggestions for further work	19
Bibliography	21

Chapter 1

Introduction

Wind energy is world wide a rapidly growing segment within the energy sector. Due to a favorable combination of high tensile strength, good wear resistance and ductility, the load bearing structural components in wind turbines are mostly made of large, complexly shaped ductile iron castings. The high ductility and toughness are of paramount importance for these castings because of the harsh weather conditions to which they may be exposed. The majority of wind turbine parts are made out of the challenging ductile iron grade EN-GJS-400-18-LT. This grade of ductile iron features the properties necessary to withstand the force of the wind and long-term exposure to the environment without failure. Moreover, the castings must exhibit high-impact strength at low temperatures [8].

Although the majority of wind turbine parts is made out of EN-GJS-400-18-LT ductile iron, only meagre information on the fatigue behavior of large EN-GJS-400-18-LT castings is available. To eliminate these shortcomings, in the four year lasting project FeVIND, launched in 2007, end users/wind turbine manufacturers, Vestas Wind Systems A/S and Siemens Wind Power A/S, joined forces with an iron foundry, Rolls-Royce Marine AS Foundry Bergen, raw material producers Elkem ASA and Tinfos Titan & Iron AS, as well as the R&D partners SINTEF and NTNU, to create a scientific lift in the production and reliable fatigue design of cast iron components for wind turbines.

The FeVIND project consists of 4 subgroups. This thesis is based on the results which were obtained in “Fatigue & Defects” subgroup. This thesis presents probabilistic and defect tolerant fatigue assessment of wind turbine castings.

1.1 Objective

The objective of this work has been to provide a database and design methodology for the reliable fatigue design of highly loaded heavy-section cast components of large future wind turbines.

1.2 Motivation

Wind turbine manufacturers have to compete with other sources of energy such as natural gas and coal. In order to produce cheaper wind electricity, larger, lighter, more efficient and less expensive wind turbines have to be developed. This is the most important challenge for the wind turbine manufacturers. EN-GJS-400-18-LT castings make up most of the weight of a modern wind turbine [8]. To have larger, lighter, more efficient and less expensive wind turbines, the cast components should be optimized with respect to fatigue life. Thus good knowledge of fatigue behavior and fatigue design of large EN-GJS-400-18-LT castings is required.

1.3 Short summary of the thesis

This dissertation consists of an introduction and seven appended papers [1-7].

The current design of large wind turbine castings against fatigue is usually based on the safe-life design approach. In the safe-life design, $P - S - N$ curves derived from fatigue testing on baseline material are required. To this end, 9 ton of EN-GJS-400-18-LT in the shape of casting blocks with two different thicknesses, 95 mm and 150 mm, was provided by the project partners. This EN-GJS-400-18-LT was investigated by means of 3D X-ray computed tomography and no defect larger than 0.2 mm was found in the material. Thus, it was supposed that this material is representative of baseline EN-GJS-400-18-LT. To establish the required $P-S-N$ diagrams for safe-life design of wind turbine castings, fatigue specimens with different dimensions machined from baseline casting blocks with different thicknesses. Constant amplitude axial fatigue tests were performed on these specimens at room temperature at $R = 0$ and $R = -1$. Geometrical size effect, wall-thickness effect (technological size effect) and mean stress effect on fatigue strength of baseline EN-GJS-400-18-LT material were evaluated and analyzed. Statistical analysis of fatigue data was done by means of the Weibull distribution, and $P-S-N$ diagrams were established. Weibull's weakest-link method was used to evaluate the size effect. Chapter 2, presents the obtained fatigue test results and their analysis for baseline EN-GJS-400-18-LT.

To study damage tolerant design of wind turbine castings, a rejected wind turbine hub was flame cut to several blanks and several defective fatigue specimens were machined from these blanks. Constant amplitude axial fatigue tests were performed on these specimens at room temperature at $R = 0$ and $R = -1$. Fatigue strength of baseline EN-GJS-400-18-LT was compared with that of defective material from the rejected wind turbine hub. The effect of graphite nodules and defects type, shape, size and position on fatigue strength of defective material was evaluated. The hypothesis that the endurance observed in an $S - N$ test can be predicted based on the analysis of crack growth from casting defects through defect-free 'base' material was tested for the analyzed defective material in this research. Chapter 3, shows the obtained results and their analysis for defective EN-GJS-400-18-LT.

To perform random defect analysis of wind turbine castings, establish the scatter of fatigue life and obtain the probability of failure of these components, 3D X-ray computed tomography was used to detect defects in defective specimens and find the defect size distribution and density of defects (number of defects per unit volume). The obtained defect size distribution and density for the defective material was used in random defect analysis to establish the scatter of fatigue life for defective specimens. Chapter 3, shows the application of 3D X-ray computed tomography in detecting defects and obtaining defect distribution in defective material to be used in random defect analysis and establishment of fatigue life scatter.

Finally, chapter 4 shows the comparison of safe-life design with damage tolerant design method in fatigue design of large wind turbine castings.

Chapter 2

Safe life design

The current design of heavy section wind turbine cast components is based on safe life design philosophy. In the safe life design, $S - N$ curves are derived from fatigue testing on baseline material and these curves are used in fatigue design of the components. Thus, to optimize heavy-section wind turbine cast components with respect to fatigue life, good knowledge of the fatigue behaviour of the material is required as a first step. Although the majority of wind turbine parts is made out of EN-GJS-400-18-LT ductile iron, only meagre information on the fatigue properties of EN-GJS-400-18-LT is available for the required range of endurance.

It is a well known phenomenon that the fatigue strength of a material decreases with increasing specimen size (size effect) [9-11]. In most materials, fatigue initiates from mechanical discontinuities, that may be considered as micro-cracks. By increasing the volume of a component, the probability of failure within a prescribed number of cycles at a given stress level increases due to the higher probability of finding a critical micro-crack. Moreover, the size of the critical defect increases with increasing size of the component. Size effect shall be taken into account in the design of large wind turbine cast components. Specimens with different sizes but from castings with the same cooling rate, show different fatigue strength (geometrical size effect).

The morphology of the graphite in cast iron significantly influences the mechanical properties [12-15]. By increasing the casting thickness, the cooling rate decreases and the nodularity and nodule count of the microstructure decreases. This yields a decrease in fatigue strength (technological size effect). Specimens with the same geometry, but from the castings with different cooling rates show different fatigue strength (technological size effect).

To apply the experimentally obtained $S - N$ curves in fatigue design of heavy section wind turbine cast iron components, both geometrical and technological size effect should be considered. But there is no robust methodology to apply the appropriate factors to $S - N$ curves to take into account both geometrical and technological size effect. Therefore, large reduction factors are usually applied to $S - N$ curves based on laboratory-size specimens to take into account size effect. This yields over design of these components. To counter this problem and eliminate uncertainties in fatigue design of large wind turbine cast iron components, it is recommended to perform fatigue testing on fatigue specimens with the dimensions and thicknesses close to heavy section wind turbine cast iron components.

To obtain the fatigue strength of the EN-GJS-400-18-LT and evaluate both geometrical size effect and wall thickness effect (technological size effect) on fatigue strength of this material, a test plan was established. Table 2.1 shows this test plan. To evaluate geometrical size effect, specimens with different dimensions from castings with the same thickness were tested. Also to evaluate wall thickness effect, specimens with the same dimensions but from castings with different thicknesses were tested. To obtain the load ratio effect, specimens with the same geometry and from the same castings were tested at different load ratios.

Table 2.1: Plan for testing baseline material.

Initial casting block thickness	Specimen cross section	Load ratio
95 mm (T95)	21 mm ($\varnothing 21$)	$R = -1, R = 0$
95 mm (T95)	50 mm ($\varnothing 50$)	$R = -1$
150 mm (T150)	21 mm ($\varnothing 21$)	$R = -1$
150 mm (T150)	120 mm \times 140 mm	$R = -1$

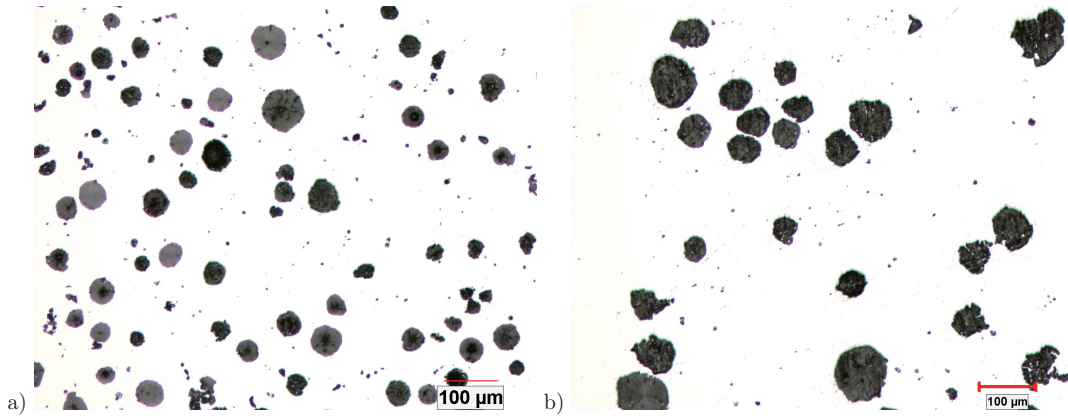


Figure 2.1: Representative optical micrograph of the EN-GJS-400-18-LT test material a) cast blocks with 95 mm thickness b) cast blocks with 150 mm thickness.

2.1 Experimental procedure

2.1.1 Material and specimens

The material under investigation was EN-GJS-400-18-LT ductile cast iron with graphite nodules contained within a ferritic matrix. In order to find the wall thickness effect on fatigue strength of the material, two types of castings with 95 mm thickness, T95, and 150 mm thickness, T150, were evaluated. Fig. 2.1 shows representative optical micrograph of the EN-GJS-400-18-LT test material.

2.1.1.1 T95 material

Mechanical properties and chemical composition of the test material were given in paper 1 [1]. The cast block dimensions were 750 mm \times 200 mm \times 95 mm. Two series of specimens were machined from these cast blocks, specimens with 21 mm diameter, $\varnothing 21$, and specimens with 50 mm diameter, $\varnothing 50$. $\varnothing 21$ specimens were tested at load ratios $R = -1$ and $R = 0$, but $\varnothing 50$ specimens were just tested at load ratio $R = -1$. Experimental procedure, fatigue test results and detail drawings of $\varnothing 21$ and $\varnothing 50$ specimens were presented in paper 1 [1].

2.1.1.2 T150 material

Mechanical properties and chemical composition of the test material were given in paper 2 [2]. The cast block dimensions were 150 mm \times 300 mm \times 1550 mm. Two series of specimens were machined from these cast blocks, specimens with 21 mm diameter, $\varnothing 21$, and heavy section specimens with 120 mm \times 140 mm cross section. All

specimens were tested at load ratio $R = -1$. Experimental procedure, fatigue test results and detail drawings of $\varnothing 21$ and $120 \text{ mm} \times 140 \text{ mm}$ specimens were presented in paper 2 [2].

2.2 Statistical analysis of fatigue data

If a large number of identical test pieces are run until fatigue failure, the number of cycles sustained will differ from specimen to specimen. The probability of failure, P , has to be introduced and connected with the applied stress, σ , and the number of cycles to failure, N . These three parameters can be expressed in a $P-S-N$ diagram. This contains a family of $S-N$ curves, each curve corresponding to a particular value of the probability of failure, P .

2.2.1 Average $S-N$ curve

In this research, the $S-N$ curve was assumed to follow the Basquin equation

$$\sigma_a = \sigma'_f (2N_f)^{-\frac{1}{m}} \quad , \quad (2.1)$$

where σ'_f is the fatigue strength coefficient and $-1/m$ the fatigue strength exponent. This curve will be a straight line on a log-log plot and may be found by linear regression analysis of fatigue data points.

2.2.2 Linear regression to find the Basquin exponent

Standard $S-N$ diagrams found in most design texts are plotted with stress (independent variable) on the ordinate and number of cycles to failure (dependent variable) on the abscissa. The standard approach in curve fitting is to assume that the parameter plotted on the abscissa is the independent variable and that plotted on the ordinate is the dependent variable. But it should be noted that with fatigue data, stress is actually the independent variable and should be treated as such in the regression analysis. To treat cycles as the independent variable can lead to errors in the regression.

Papers 1 and 2 [1, 2] show the linear regression analysis which was used to find the average $S-N$ curves for tested specimens. The obtained average $S-N$ curves for T95 and T150 material are presented in papers 1 and 2 [1, 2] and also figures 2.2 and 2.3, respectively. The possible reason for different slopes of $S-N$ curves in Fig. 2.3 is explained in paper 2 [2]

2.2.3 Weibull fatigue life distribution

To establish $P-S-N$ diagram, $P-N$ relations at different stress levels should be experimentally determined. By having $P-N$ relations, it will be possible to find, for every probability of failure, its related "number of cycles to failure" at different stress levels. The two-parameter Weibull distribution was used to model the fatigue lives of the specimens tested in this research.

2.2.4 $P-S-N$ diagram

Once the fatigue life distribution is known, it will be possible to establish the $P-S-N$ diagram. Statistical analysis of all fatigue test results obtained in this research was performed and $P-S-N$ diagrams were established for all analyzed specimens.

Paper 1 [1] presents detailed statistical analysis which was performed to draw average $S-N$ curves, obtain Weibull distribution parameters and establish $P-S-N$ diagrams. $P-S-N$ diagrams for $\varnothing 21$ and $\varnothing 50$ specimens from T95 castings were presented in paper 1 [1]. $P-S-N$ diagrams for $\varnothing 21$ and $120 \text{ mm} \times 140 \text{ mm}$ heavy section specimens from T150 castings were presented in paper 2 [2].

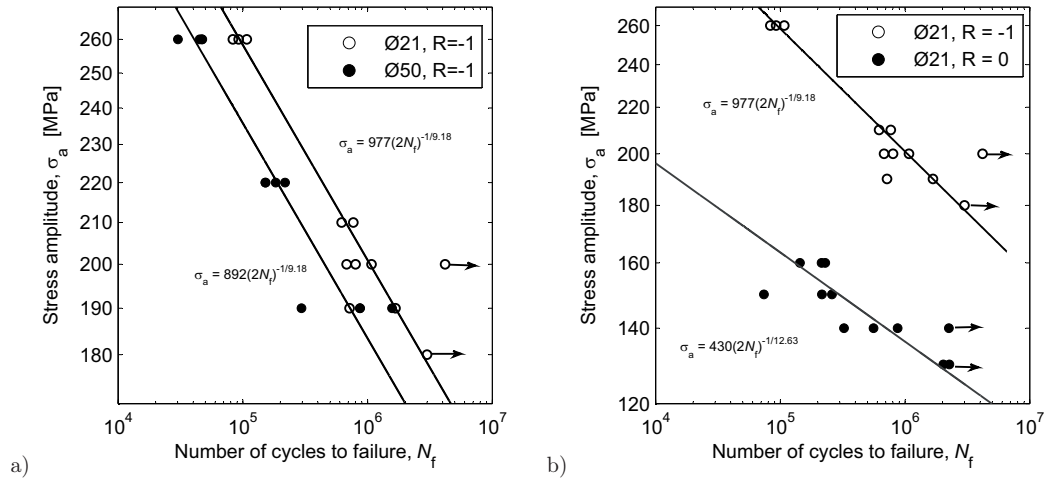


Figure 2.2: Fatigue behaviour of EN-GJS-400-18-LT cylindrical specimens machined from T95 casting blocks.

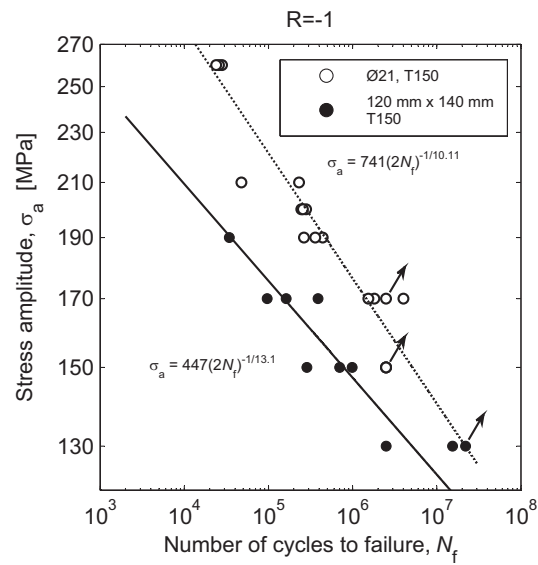


Figure 2.3: Fatigue behaviour of EN-GJS-400-18-LT cylindrical specimens machined from T150 casting blocks.

2.3 Size effect

2.3.1 Geometrical size effect

As mentioned above, the fatigue strength of materials decreases with increasing component size. In most materials, fatigue initiates from material defects. By increasing the volume (or surface) of the component, the probability of failure increases due to the higher probability of finding a critical defect. There exist empirical methods to take the size of the component into account, but these methods are generally not compatible with finite element stress analysis. These shortcomings may be eliminated by means of the Weibull's weakest-link theory and the statistics of extremes, which may be applied directly to finite element results.

In this research, Weibull's weakest-link theory was used to model the geometrical size effect and predict $P - S - N$ diagram for large specimens based on the $P - S - N$ of small specimens. Paper 1 [1] shows the detailed implementation of Weibull's weakest-link theory in modeling the geometrical size effect.

In paper 1 [1], Weibull's weakest-link theory was used to predict $P - S - N$ diagram for $\varnothing 50$ based on the $P - S - N$ of $\varnothing 21$ specimens. The predicted $P - S - N$ diagram for $\varnothing 50$ specimens was compared with experimental results. In paper 2 [2], Weibull's weakest-link method was used to predict $P - S - N$ diagram for heavy section $120 \text{ mm} \times 140 \text{ mm}$ based on the $P - S - N$ of $\varnothing 21$ specimens. The predicted $P - S - N$ diagram for $120 \text{ mm} \times 140 \text{ mm}$ specimens was compared with experimental results.

2.3.2 Technological size effect

As noticed above, the morphology of the graphite in cast iron significantly influences the mechanical properties. By increasing the casting thickness, the cooling rate decreases and the fatigue strength decreases. In ductile cast iron, by decreasing the cooling rate, the nodularity and nodule count of the microstructure decreases.

As noticed above, the fatigue test results for $\varnothing 21$ specimens from T95 blocks is presented in paper 1 [1] and for $\varnothing 21$ specimens from T150 blocks is presented in paper 2 [2]. The comparison of the fatigue test results for $\varnothing 21$ from cast blocks with 95 mm and 150 mm thicknesses was performed in paper 2 [2] and the wall thickness effect on fatigue strength was evaluated.

To evaluate microstructural effect on fatigue strength, metallography analysis was performed on broken fatigue specimens from T95 and T150 castings. Detailed explanation on metallography analysis and microstructural properties of T95 and T150 material were presented in paper 2 [2]. The microstructural properties of T95 and T150 material and their fatigue strength presented in this research may be used by wind turbine manufacturers to estimate the fatigue strength of their components based on their microstructural properties.

2.4 Mean stress effect

Clearly, service stress cycles are not always fully reversed. In order to evaluate mean stress effect on fatigue life, $\varnothing 21$ specimens from T95 castings were tested at load ratios $R = -1$ and $R = 0$. The empirical modified Goodman, Hempel (Morrow) and Walker approaches may be used to quantify the effect of mean-stress on the fatigue strength. The comparison of fatigue test results for $\varnothing 21$ specimens at $R = -1$ and $R = 0$ and quantification of load ratio effect by modified Goodman, Hempel (Morrow) and Walker approaches were presented in paper 1 [1].

Chapter 3

Damage tolerant design

The current design of large wind turbine castings against fatigue is usually based on the safe life approach. In the safe life design, fatigue testing is carried out on baseline material to produce $S - N$ curves. Since the physical phenomena behind these $S - N$ curves are not known, to apply these curves to a real component, large reduction factors must be used to account for different parameters such as stress concentration, stress gradient, fatigue scatter and also taking into account nondestructive test results such as ultrasonic inspection [16] or magnetic particle inspection [17]. As a result, in some situations, a significant portion of the useful life of the structure remains unused once it is retired and thus the structure is heavily over-designed and in some other situations, the fatigue design of the component is non-conservative and the component has premature fatigue failure. One way to safely decrease the weight of large cast components and allow these to be operated to the limits of their useful life, while maintaining safety, is to use a damage tolerant design approach.

In most cast materials, the fatigue life is controlled by the growth of cracks initiated from inclusions, nodules or other metallurgical defects such as shrinkage cavities [18-23]. Since fatigue cracks are frequently observed early in the fatigue life, it is usually assumed that the crack initiation stage is negligible and that a damage tolerant design approach can be used to predict the fatigue life of the component. In damage tolerant design, defects are considered as pre-existent cracks and fatigue life and fatigue limit are controlled by the crack propagation law and by the threshold stress intensity factor, respectively.

Due to the large dimensions and the geometrical complexity of heavy-section components used in wind turbines, defective parts are obtained quite often. The purpose of this chapter is to compare the fatigue strength of defective material with that of baseline material, presented in paper 1 [1], find the effect of defects present in these components on fatigue life and evaluate the life controlling parameters and also to test the hypothesis that the endurance observed in an $S - N$ test can be predicted based on the analysis of crack growth from casting defects through defect-free 'base' material.

To this end, a 24 ton wind turbine hub, which had been rejected by NDT, since NDT revealed impermissible defects, was flame cut into several blanks and comprehensive analysis of the defective material was performed. Paper 3 [3] shows this analysis and results. Following paragraphs in this chapter give an overview of what has been presented in paper 3 [3].

As noticed above, a 24 ton wind turbine hub, which had been rejected by NDT, was flame cut into several blanks. Fatigue specimens with 21 mm diameter were machined from these blanks. These were axially fatigue tested at room temperature at $R = 0$ and $R = -1$, and the scatter of fatigue life was established. To evaluate the influence of casting defects on the fatigue strength of this material, the fatigue test results for defective material were compared with fatigue data for baseline EN-GJS-400-18-LT, paper 1 [1], Fig. 3.1. The baseline EN-GJS-400-18-LT was investigated by means of XCT and no defect larger than 0.2 mm was found in the material. The baseline test specimens had the same geometry as the specimens of the present study. Fig. 3.1 a and b show comparisons between the two material qualities for $R = -1$ and $R = 0$.

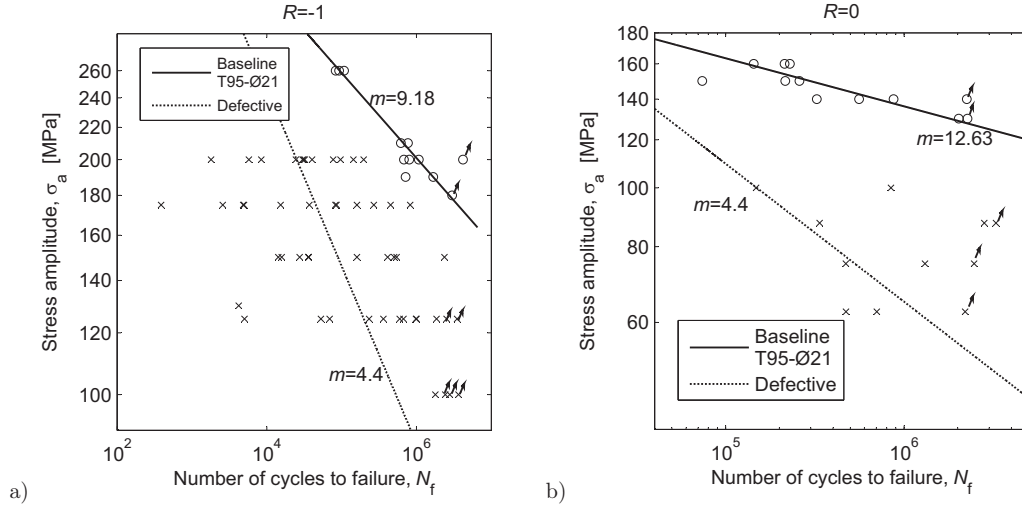


Figure 3.1: Comparison of the fatigue strength of defective (rejected) material with baseline material at a) $R = -1$, b) $R = 0$ (arrows denote run-outs).

To evaluate life controlling parameters, fractography and metallography of broken specimens were performed and type, position and size of the fatigue crack initiating defects and several important microstructural parameters such as nodularity and nodule count of the graphite nodules were determined and measured. In all analyzed specimens fatigue crack was initiated from shrinkage cavities. The only other effective defects, beside shrinkage cavities, were Mg inclusions.

The specimens were divided into 6 groups based on their fatigue crack initiation site:

- Group 1: Fatigue crack was initiated from a single surface or sub-surface shrinkage cavity, Fig. 3.2a.
- Group 2: Fatigue crack was initiated from a cluster of surface or sub-surface shrinkage cavities, Fig. 3.2b.
- Group 3: Fatigue cracks were initiated from different defects in different areas simultaneously, Fig. 3.2c.
- Group 4: Fatigue crack was initiated from an internal shrinkage cavity, Fig. 3.2d.
- Group 5: Fatigue crack was initiated from a shrinkage cavity but fatigue crack propagation was favored by Mg inclusions, Figures 3.2e.
- Group 6: Fracture surface of the specimens is totally covered with porosities, Fig. 3.2f. Specimens of this group showed very low fatigue strength. Most of the data-points on the left side of the Figures 3.1a and 3.1b are from this group.

The position and size of the fatigue crack initiating defects were measured in fractography analysis. The measured size and position of defects in conjunction with stress distribution in each specimen was used to predict the fatigue life for each specimen. To perform fatigue crack growth simulations and predict the fatigue life, an in-house finite element post-processor, **P•FAT**, was used [24, 25]. The estimated fatigue lives were compared with the experimental results and the influence of defect type, size, shape and position on the fatigue strength of EN-GJS-400-18-LT was investigated. Fig. 3.3 shows the comparison of the predicted fatigue lives

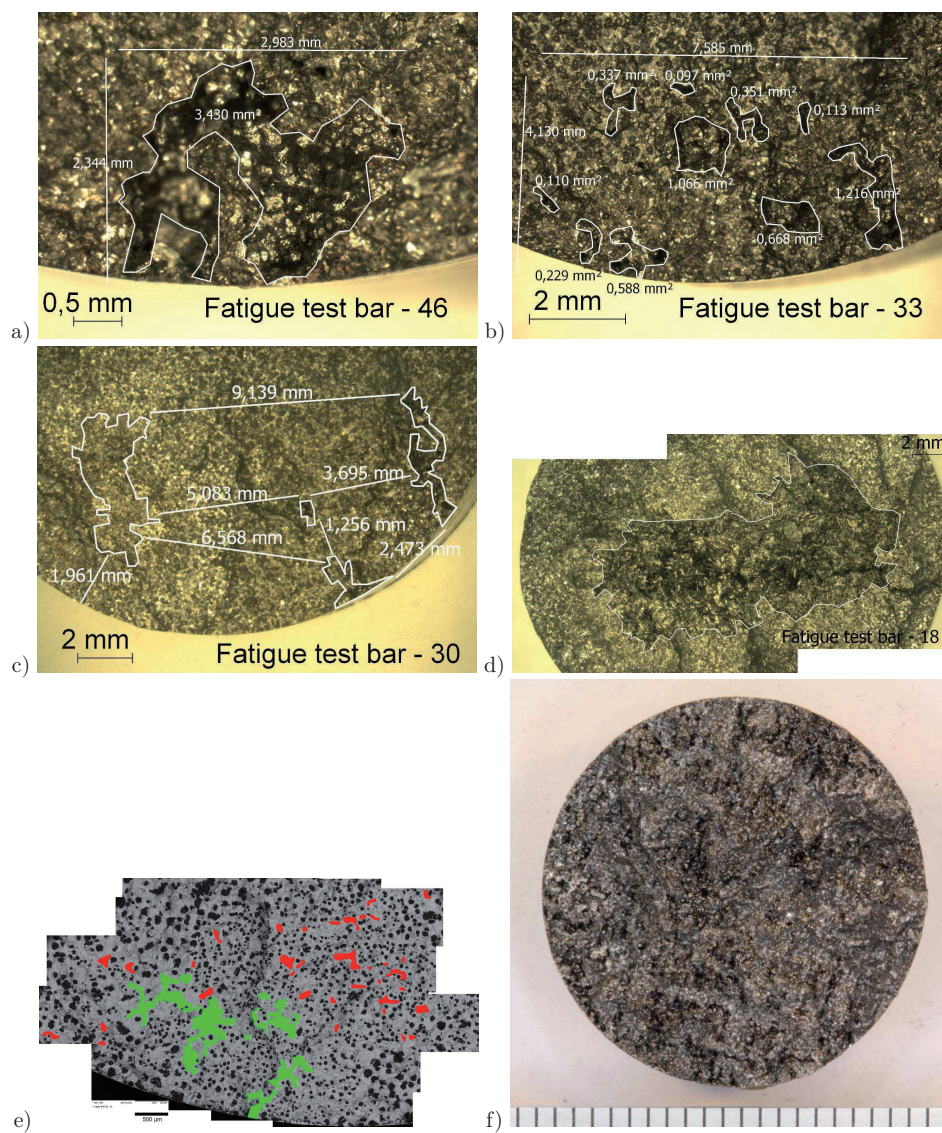


Figure 3.2: Fatigue crack initiation site, a) Group 1, b) Group 2, c) Group 3, d) Group 4, e) Group 5: Red areas are Mg oxide and green areas are shrinkage cavities, f) Group 6.

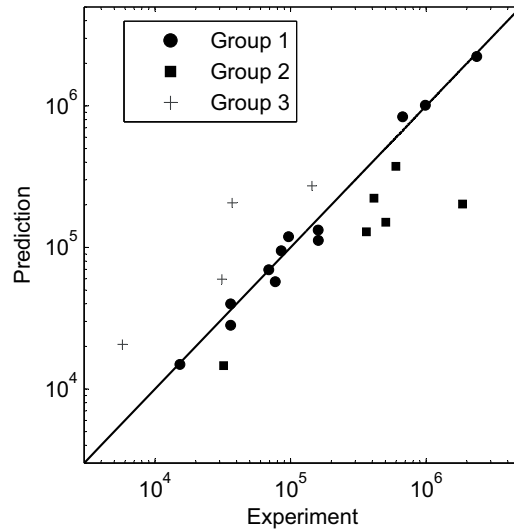


Figure 3.3: Comparison of predicted fatigue lives with experimental results.

with experimental results for specimens contained in groups 1, 2 and 3. A more detailed assessment of the analysis and experimental observations for the different specimen categories was given in paper 3 [3].

The fatigue crack path in material was evaluated and the influence of graphite nodules on fatigue crack growth was discussed. Finally, the endurance of defective EN-GJS-400-18-LT material was compared with the baseline material, Fig. 3.1, and it was shown that the slope of $S - N$ curve for baseline material is different than the slope of $S - N$ curve for defective material. As noticed above, due to the large dimensions and the geometrical complexity of heavy-section components used in wind turbines, defective parts are obtained quite often. The current design of large wind turbine cast components is based on $S - N$ curves obtained for baseline material, while the real slope of $S - N$ curves for large defective components is different.

3.1 Random defect analysis

The analysis on defective specimens from the rejected wind turbine hub showed that crack initiation stage is negligible and fatigue life is controlled by the crack propagation law. It is well known that fatigue test results are scattered, Fig. 3.1. In order to model this scatter and find the probability of failure of the components, damage tolerant design in conjunction with defects distribution may be considered for fatigue life estimation in a random defect analysis.

The main steps for obtaining the fatigue life distribution of a component can be summarized as follows:

1. Develop a three dimensional FE model and perform a stress analysis of a component using a standard finite element program.
2. Drawing defects distribution inside the part.
3. Calculate the maximum principal stress for all defects and find the life controlling defects.

4. Perform fatigue crack growth calculations.
5. Repeat steps 2–4 for a large number of nominally equal components to obtain the fatigue life distribution of the component.

By repeating the foregoing analysis for a large number of nominally equal components (Monte Carlo simulation), the fatigue life distribution of the component is obtained. Thus, the designer will be able to find the probability of fatigue failure.

Hence, every effort in order to try and predict scatter of fatigue life for cast materials requires a sound characterization of the defect size distribution and defects density, number of defects per unit volume of material. Classically, such a distribution can be obtained from serial two dimensional metallographic observations. However, the amount of material that can be studied by such a tedious method is generally very low. Predictions of the three dimensional maximum defect size from two dimensional method sometimes involve errors [26]. For instance, parameters like the statistical size or shape distribution of the pores are rather difficult to obtain precisely. Sometimes material includes mixture of two different types of defects. The character of this mixed distribution is that as the number of inspections and the size of the inspection area increases, it is more likely to pick out the presence of the second particle type, which rarely occurs and leads to final fatigue failure. In these cases, most times the limited volume of material inspected by conventional methods does not let to catch second type of particles which has large size but rare population [27]. Conventional approaches only provide two dimensional information of defects, such as pores, which may not adequately describe their tortuous three dimensional morphology.

These shortcomings may be eliminated by use of 3D X-ray computed tomography to find defect distribution in material. High resolution X-ray tomography is a technique that can be used to visualize the internal structure of materials.

Recent developments in high resolution X-ray tomography allowed three dimensional characterization of porosity. Most efforts in characterization of defect distribution in cast parts using 3D X-ray computed tomography are limited to miniature parts with maximum size of about 3 mm. In large cast components some areas include defects in order of 2 millimeter. To obtain the correct distribution of defects in large cast parts it is essential to evaluate a large volume of these parts. Papers 4 and 5 [4, 5] show how X-ray tomography was used in this research to obtain defect distribution in large parts. Fig. 3.4 shows a view of defects detected by this method in one of the $\varnothing 21$ specimens from the rejected wind turbine hub. Papers 4 and 5 [4, 5] also show how such statistical results can be used to perform random defect analysis and predict fatigue behaviour of large cast components, establish the scatter of fatigue life and predict the probability of failure of components. Fig. 3.5 shows the established scatter of fatigue lives for $\varnothing 21$ specimens by random defect analysis based on defects size distribution obtained from 3D X-ray computed tomography.

Paper 6 [6], shows how the obtained defect size distribution can be used to predict geometrical size effect.



Figure 3.4: Defects detected by 3D X-ray computed tomography (XCT) in a fatigue specimen from a rejected wind turbine hub.

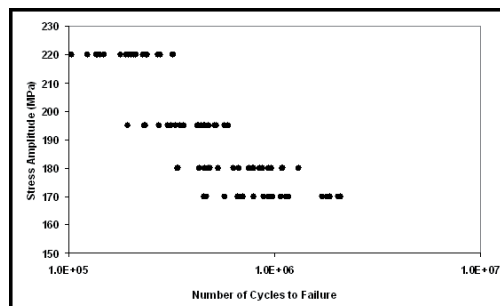


Figure 3.5: Predicted fatigue life distribution

Chapter 4

Comparison of safe life design with damage tolerant design

This chapter evaluates the transition from safe life design to damage tolerant design of heavy section wind turbine cast iron components by comparing the safe life design to damage tolerant design of these components. In chapter 2, the required $P-S-N$ curves for safe life design of large wind turbine castings were established. Since the physical phenomena behind these $S-N$ curves are not known, to apply these curves to a real component, large reduction factors must be used to account for different parameters such as defects. As a result, in some situations, a significant portion of the useful life of the structure remains unused once it is retired and thus the structure is heavily over-designed and in some other situations, the fatigue design of the component is non-conservative and the component has premature fatigue failure. To counter these drawbacks, damage tolerant design of large wind turbine castings was evaluated in chapter 3.

One of the main goals of this research, besides establishing the reliable database of the material, is to develop reliable engineering methods for prediction of the endurance of wind turbine large cast components containing defects. Both safe life and damage tolerant methodologies were evaluated in this research. But in order to come up with robust conclusions and recommendations on the use of these two methods in fatigue design of large wind turbine castings, the comparison of these two methods for fatigue design of a heavy section wind turbine casting is required.

To this end, safe life design of a 750 mm x 200 mm x 95 mm EN-GJS-400-18-LT ductile cast iron block, Fig. 4.1, representative of heavy section wind turbine cast iron components, was compared with damage tolerant design of the block. This helped to reveal the limitation of safe life design method in design of large wind turbine castings and showed the application of damage tolerant design based on the non-destructive test results in design of these castings. Paper 7 [7] shows this comparison and the final conclusions. Following paragraphs in this chapter give an overview of what has been presented in paper 7 [7].

Although the majority of wind turbine parts is made out of EN-GJS-400-18-LT ductile iron, only meagre information on the fatigue properties of EN-GJS-400-18-LT is available, thus some of the wind turbine manufacturers use the synthetic $S-N$ curves instead of laboratory based $S-N$ curves. In order to safe life design of the representative casting shown in Fig. 4.1, synthetic $S-N$ curves at load ratios of $R = -1$ and $R = 0$ were established for the analyzed cast block by following the methodology given in Ref. [28]. The developed synthetic $S-N$ curves were compared with experimentally determined $S-N$ curves of baseline EN-GJS-400-18-LT at $R = -1$ and $R = 0$. Synthetic $S-N$ curves agree fairly well with experimentally determined $S-N$ curves at $R = -1$, but not at $R = 0$.

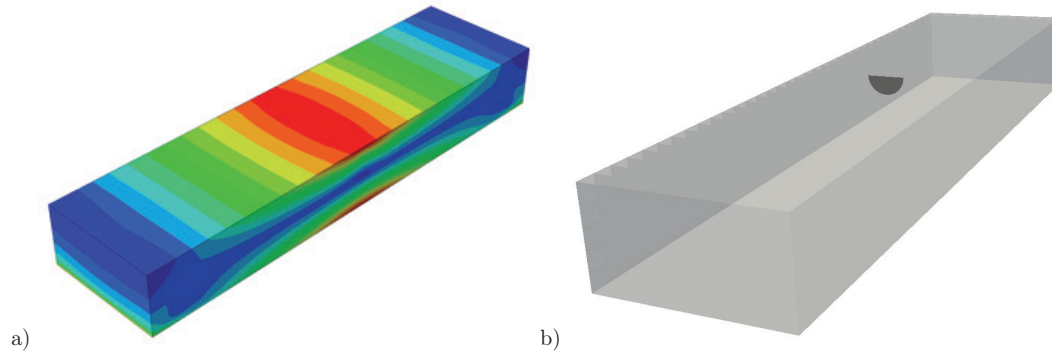


Figure 4.1: Cast 750 mm \times 200 mm \times 95 mm block subjected to three-point bending a) surface stress distribution b) representative semi-elliptical surface crack.

Then, it was assumed that the analyzed cast block contains a semi-circular surface defect with 5 mm diameter. To take into account the effect of a 5 mm diameter semi-circular surface defect on fatigue strength, a reduction factor based on Ref. [29] was applied to the obtained synthetic $S - N$ curve, and the reduced synthetic $S - N$ curve for the analyzed cast block with defect was established.

For damage tolerant design of the representative casting shown in Fig. 4.1, fatigue crack growth analysis was performed at different loads to establish $S - N$ curves for the analyzed cast block with a 5 mm diameter semi-circular surface defect.

Fig. 4.2 shows the comparison of reduced synthetic $S - N$ curve with fatigue crack growth based $S - N$ curve for the analyzed cast block containing a semi-circular surface defect with 5 mm diameter under axial loading.

The comparison of reduced synthetic $S - N$ curve with fatigue crack growth based $S - N$ curve shows that reduced synthetic $S - N$ curves over-estimate the fatigue strength of defective EN-GJS-400-18-LT components. On the other hand, after application of defect reduction factor, S_d , to synthetic or experimentally determined $S - N$ curves, they still show higher fatigue strength for defective material than what it is. This is due to different slopes of $S - N$ curves for baseline clean and defective EN-GJS-400-18-LT. In paper 7 [7], it was tried to explain the difference between the slopes of $S - N$ curves for baseline and defective material by considering the sizes of defects contained in material and the subsequent fatigue mechanism.

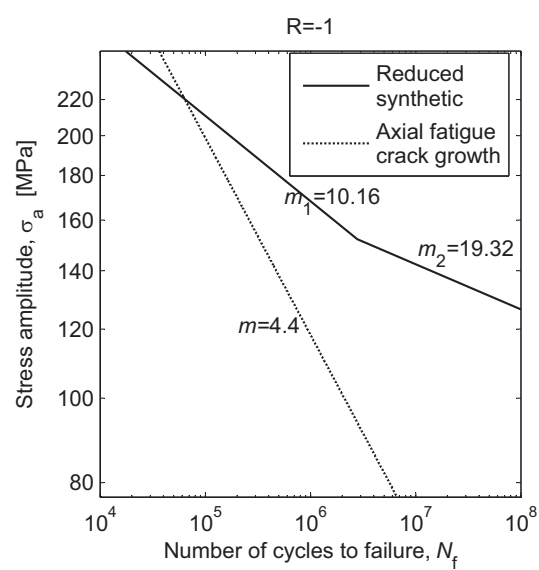


Figure 4.2: Comparison of reduced synthetic $S - N$ curve with axial fatigue crack growth based $S - N$ curve for the 750 mm \times 200 mm \times 95 EN-GJS-400-18-LT cast block contains a semi-circular surface defect with 5 mm diameter.

Chapter 5

Conclusions and suggestions for further work

The objective of this thesis has been to establish the required database and design methodology for reliable fatigue design of heavy-section wind turbine cast components of the future.

$P - S - N$ diagrams for baseline EN-GJS-400-18-LT were established. Geometrical size effect, technological size effect and also load ratio effect on fatigue strength of this material were evaluated. Heavy-section fatigue specimens, representative of large wind turbine castings, were fatigue tested in the required range of fatigue endurance of wind turbine castings.

Defects present in large wind turbine castings were realized and effect of defects type, size, shape and position on fatigue strength of EN-GJS-400-18-LT were evaluated. The application of fatigue crack growth analysis in prediction of fatigue life for defective wind turbine castings was tested. Defect distribution in defective material was obtained by the use of 3D X-ray computed tomography and the obtained defect distribution was used in a random defect analysis to establish the scatter of fatigue lives for defective specimens.

Finally application of the obtained results in safe-life and damage tolerant design of large wind turbine castings were presented and compared.

There are still some items which are left untreated in this thesis. From material database point of view, some suggestions for further work are:

- Evaluating the effect of chunky graphite on fatigue strength of EN-GJS-400-18-LT, evaluating the possibility of modeling area covered with chunky graphite as a crack.

During fatigue testing of baseline material, 3 of the specimens showed much lower fatigue life than others. The fractography analysis showed presence of chunky graphite at fatigue crack initiation site and specimen's fracture surface. Due to the fact that just few specimens had chunky graphite at their fracture surface, it was not possible to reach to a robust conclusion on the effect of chunky graphite on fatigue strength of this material. Although there are also some reports on the effect of chunky graphite on fatigue strength of GJS-400 cast iron [30], but the author could not reach to a robust and reliable conclusion by reviewing the available reports. One possibility to model the effect of chunky graphite on fatigue strength, is to consider the area covered with chunky graphite as a crack with the same size. But before the application of this methodology in fatigue design of large wind turbine castings, it should be tested and verified.

- Realizing surface and sub-surface effective defects on as-cast surface of large EN-GJS-400-18-LT components and their effect on fatigue life.

Defective fatigue specimens tested in this research, were machined from blanks which were flame cut from

a rejected wind turbine hub. Thus, they did not contain casting surface and subsequently surface and sub-surface defects which are present on as-cast surface. Although, most highly loaded areas on large wind turbine castings are machined and does not contain casting surface, but however evaluating these kinds of defects seems essential for optimum design of these castings. There are also some reports on the effect of as-cast surface defects on fatigue strength of GJS-400 cast iron [30], but the author could not reach to a robust and reliable conclusion by reviewing the available reports. To this end, performing 4-point bending fatigue tests on the blanks with as cast surface, machined from large wind turbine castings, is recommended.

- Evaluating the fatigue crack growth behaviour of EN-GJS-400-18-LT in vacuum.

It was observed in this research and some other researches [3, 22, 23] that environment has a strong influence on the fatigue crack growth behaviour in nodular cast iron and that crack growth rate is 5 to 20 times higher in air than in vacuum. In order to model and predict the fatigue life of cast components containing internal defects, the fatigue crack growth behaviour of EN-GJS-400-18-LT in vacuum is required.

From simulation point of view, some suggestions for further work are:

- Modeling the interaction between single cracks and the subsequent joining of them and the formation of a new, larger crack.

It was observed in this research [3], when there are some defects relatively close together at the specimens surface and sub-surface, the fatigue life of the specimen dropped. Presence of relatively close defects on the component surface or sub-surface can be observed by non-destructive tests such as magnetic particle inspection, but there is no robust and reliable methodology to predict the effect of these relatively close defects on fatigue strength of the component. According to Ref. [16] defects in ductile cast iron core zone are allowed to be about 15 times larger than defects in rim zone, at different defect's severity levels. It was also shown in this research that in some cases the fatigue cracks were initiated from small surface defects despite the presence of large internal defects. This is why evaluation of internal defects is less important than the surface and sub-surface defects.

Bibliography

- [1] M. Shirani, G. Härkegård, Fatigue life distribution and size effect in ductile cast iron for wind turbine components. *Eng Fail Anal* 18 (2011) 12-24
- [2] M. Shirani, G. Härkegård, Large scale axial fatigue testing of ductile cast iron for heavy section wind turbine components, submitted to *Eng Fail Anal*.
- [3] M. Shirani, K. M. Pedersen, G. Härkegård, Fatigue life prediction of heavy-section wind turbine components made of ductile cast iron containing casting defects , submitted to *Fatigue & Fracture of Engineering Materials & Structures*.
- [4] M. Shirani, G. Härkegård, Fatigue Crack Growth Simulation in Components with Random Defects, *Journal of ASTM International* 6 (9).
- [5] M. Shirani, G. Härkegård, Damage Tolerant Design of Cast Components Based on Defects Detected by 3D X-ray Computed Tomography, Submitted to the Special Issue 'Fatigue Design & Material Defects' of the *International Journal of Fatigue*.
- [6] M. Shirani, G. Härkegård, N. Morin, Fatigue life prediction of components made of spheroidal graphite cast iron, *Procedia Engineering* 2 (2010) 1125–1130.
- [7] M. Shirani, G. Härkegård, From Safe Life to Damage Tolerant Design of Wind Turbine Castings, submitted to *Wind Energy*.
- [8] H. Roedter, M. Gagne, Ductile Iron for Heavy Section Wind Mill Castings: A European Experience, *Proceedings of the 2003 Keith D. Millis World Symposium on Ductile Iron*, South Carolina, 2003; paper 11.
- [9] Phillips C, Heywood R. The size effect in fatigue of plain and notched steel specimens loaded under reversed direct stress. *Proc Inst Mech Eng* 1951;165:113–24.
- [10] Gaenser H. Some notes on gradient, volumetric and weakest link concepts in fatigue. *Comput Mater Sci* 2008;44(2):230–9.
- [11] Carpinteri A, Spagnoli A, Vantadori S. Size effect in S–N curves: a fractal approach to finite-life fatigue strength. *Int J Fatigue* 2009;31(5):927–33.
- [12] P. Emerson, W. Simmons, Final Report on the Evaluation of Graphite Form in Ferritic Ductile Irons by Ultrasonic and Sonic Testing and on the Effect of Graphite Form on Mechanical Properties, *AFS Trans* 84 (1976) 109-128.
- [13] G. Ru, B. Doshi, Relationship Between Mechanical Properties and Graphite Structure in Cast Irons. II. Ductile Iron, *Modern Casting* 70 (7) (1980) 70-74.

-
- [14] H. Itofuji, K. Kawamura, N. Hashimoto, H. Yamada, Production and Evaluation of Heavy- Section Ductile Cast Iron, Transactions of the American Foundrymen's Society. 98 (1990) 585-595.
- [15] C. Loper Jr, Evaluation of Microstructural Factors Affecting Heavy-Section Ferritic DI Castings, in: Ninety-Fifth Annual Meeting American Foundrymen's Society, 1991, pp. 543-549.
- [16] EN 12680-3:2003. Founding - Ultrasonic examination, Part 3: Spheroidal graphite cast iron castings, CEN, August 2003.
- [17] EN 1369:1997. Founding - Magnetic particle inspection, CEN, July 1997.
- [18] P. Clement, J. Angeli, A. Pineau, Short crack behaviour in nodular cast iron, Fatigue & Fracture of Engineering Materials & Structures 7 (4) (1984) 251-265.
- [19] K. Tokaji, T. Ogawa, Fatigue life distribution and its simulation in spheroidal graphite cast irons, Zairyo 44 (497) (1995) 187-193.
- [20] T. Palin-Luc, S. Lasserre, Y. Berard, Experimental investigation on the significance of the conventional endurance limit of a spheroidal graphite cast iron, Fatigue & Fracture of Engineering Materials & Structures 21 (2) (1998) 191-200.
- [21] H. Agha, A. Béranger, R. Billardon, F. Hild, High-cycle fatigue behaviour of spheroidal graphite cast iron, Fatigue & Fracture of Engineering Materials & Structures 21 (3) (1998) 287-296.
- [22] M. Nadot, B. Ranganathan, Fatigue life assessment of nodular cast iron containing casting defects, Fatigue & Fracture of Engineering Materials & Structures 22 (4) (1999) 289-300.
- [23] Y. Nadot, J. Mendez, N. Ranganathan, Influence of casting defects on the fatigue limit of nodular cast iron, International Journal of Fatigue 26 (3) (2004) 311-319.
- [24] A. Wormsen, A. Fjeldstad, G. Härkegård, A post-processor for fatigue crack growth analysis based on a finite element stress field, Computer Methods in Applied Mechanics and Engineering 197 (6-8) (2008) 834-845.
- [25] A. Fjeldstad, A. Wormsen, G. Härkegård, Simulation of fatigue crack growth in components with random defects, Eng Fract Mech 75 (5) (2008) 1184-1203.
- [26] G. Shi, H.V. Atkinson, C.M. Sellars, C.W. Anderson, Application of the Generalized Pareto Distribution to the Estimation of the Size of the Maximum Inclusion in Clean Steels, Acta Materialia 47 (1999) 1455-1468.
- [27] S. Zhou, Y. Murakami, S. Beretta, Y. Fukushima, Experimental Investigation on Statistics of Extremes for Three-Dimensional Distribution of Non-metallic Inclusions, Materials Science and Technology 18 (2002) 1535-1543.
- [28] H. Gudehus, H. Zenner, Leitfaden für eine Betriebsfestigkeitsberechnung, 4th Edition, Verlag Stahleisen, Düsseldorf 1999.
- [29] G. Lloyd, Guideline for the certification of wind turbines, Germanische Lloyd, Hamburg, Germany (2010).
- [30] Kaufmann H, Wolters D. Zyklische beanspruchbarkeit dickwandiger bauteile aus ferritischem gueisen mit kugelgraphit. Konstruieren Giessen 2002;27(1):427.

Paper 1



Contents lists available at ScienceDirect

Engineering Failure Analysis

journal homepage: www.elsevier.com/locate/engfailanal

Fatigue life distribution and size effect in ductile cast iron for wind turbine components

M. Shirani *, G. Härkegård

Norwegian University of Science and Technology, Dept. of Engineering Design and Materials, NO-7491 Trondheim, Norway

ARTICLE INFO

Article history:

Received 23 May 2010
 Received in revised form 24 July 2010
 Accepted 26 July 2010
 Available online 30 July 2010

Keywords:

EN-GJS-400-18-LT
 Fatigue strength
 Statistical analysis
 Weakest-link theory
 Size effect

ABSTRACT

The present paper deals with the experimental determination and statistical analysis of high cycle fatigue properties of EN-GJS-400-18-LT ductile cast iron. Constant amplitude axial fatigue tests were performed at room temperature at $R = 0$ and $R = -1$. In order to evaluate the size effect, fatigue tests were carried out on two sets of specimens with different dimensions. The specimen diameters were 21 mm and 50 mm. Statistical analysis of fatigue data was done by means of the Weibull distribution, and $P-S-N$ diagrams were established. The established $P-S-N$ diagrams showed that the Weibull distribution is well fit to the scatter of the experimentally obtained fatigue life data. Weibull's weakest-link method was used to evaluate the size effect. It made a satisfactory prediction of the fatigue strength for specimens with different dimensions.

© 2010 Elsevier Ltd. All rights reserved.

1. Introduction

Wind power is presently the world's fastest growing source of energy. For the next twenty years it is expected to expand at double-digit rates. Metal components make up nearly 90% of the weight of a modern wind turbine. Due to a favorable combination of high tensile strength, good wear resistance and ductility, the load bearing structural components in wind turbines are mostly made of large, complexly shaped ductile iron castings. Cast iron is typically used for the rotor hub, forward housing or frame, gearbox housing and bearing housings. Depending on the size of the turbine, a single wind turbine contains 10–25 tons of ductile iron.

The high ductility and toughness are of paramount importance for these castings because of the harsh weather conditions to which they may be exposed. The majority of wind turbine parts are made out of the challenging ductile iron grade EN-GJS-400-18-LT. This grade of ductile iron features the properties necessary to withstand the force of the wind and long-term exposure to the environment without failure. Moreover, the castings must exhibit high-impact strength at low temperatures [1].

For wind power to become competitive compared to other sources of energy, larger, more efficient and less expensive wind turbines have to be developed. Cast components make up much of the weight of the wind turbine. To develop larger and more powerful wind turbines, lighter cast components are required. The cast components should be optimized with respect to fatigue life.

The current design of large wind turbine castings against fatigue is usually based on the safe life design approach. In the safe life design, fatigue testing is carried out on baseline material to produce $S-N$ curves. In order to apply these $S-N$ curves to a real wind turbine cast component, reduction factors must be used to account for different parameters such as stress concentration, stress gradient, fatigue scatter and also taking into account nondestructive test results such as ultrasonic

* Corresponding author. Tel.: +47 735 93761; fax: +47 735 94129.
 E-mail address: mehdi.shirani@ntnu.no (M. Shirani).

inspection [2] or magnetic particle inspection [3]. The reader is referred to Ref. [4] for detailed explanation of these reduction factors.

Thus, to optimize heavy-section wind turbine cast components with respect to fatigue life, good knowledge of the fatigue behaviour of the material is required as a first step. Although the majority of wind turbine parts is made out of EN-GJS-400-18-LT ductile iron, only meagre information on the fatigue properties of EN-GJS-400-18-LT is available for the required range of endurances. The results shown in this research, to the best of the authors' knowledge, are the first published $S-N$ curves on EN-GJS-400-18-LT ductile iron. Because of the comprehensive application of ductile cast iron in the automotive industry, most experimental data have been limited to ductile cast iron grades with application to automotive components and in the very high cycle fatigue regime [5–8].

The next step in design of lighter large cast components is the application of fatigue data obtained by means of conventional fatigue testing. Test results show scatter in the fatigue life from specimen to specimen. In such a situation, it is useful to define a probability of failure, P , at a given stress level, σ . Therefore an $S-N$ curve, at an acceptable probability level, P , is required to represent the relationship between the stress amplitude, σ_a , and the endurance, N , for which less than some small percentage of specimens would fail. This $P-S-N$ curve can be found by statistical analysis of fatigue data and then be applied to lifetime calculation [9]. Fatigue analysis of large wind turbine cast components shall be performed with a recommended probability of failure, P , given in Ref. [4].

It is a well known phenomenon that the fatigue strength of a material decreases with increasing specimen size (size effect) [10–12]. In most materials, fatigue initiates from mechanical discontinuities, that may be considered as micro-cracks. By increasing the volume of a component, the probability of failure within a prescribed number of cycles at a given stress level increases due to the higher probability of finding a critical micro-crack. Moreover, the size of the critical defect increases with increasing size of the component. Size effect shall be taken into account in the design of large wind turbine cast components [4].

There exist empirical methods to take the size of the component into account, but these methods are generally not compatible with finite element stress analysis. These shortcomings may be eliminated by means of the Weibull's weakest-link theory [13–15] and the statistics of extremes, which may be applied directly to finite element results [16].

The main aim of this study is to present the fatigue properties of EN-GJS-400-18-LT ductile cast iron used widely in the wind turbine industry and to experimentally evaluate the geometrical size effect and mean stress effect on fatigue strength of this material. To this end, constant amplitude axial fatigue tests have been carried out using smooth specimens of EN-GJS-400-18-LT ductile cast iron in ambient air at load ratios of $R = 0$ and $R = -1$. To evaluate the size effect, fatigue tests were carried out on two sets of specimens with diameters 21 mm and 50 mm. Statistical analysis of the fatigue life of the specimens was done using the Weibull distribution, and $P-S-N$ diagrams were established. Weibull's weakest-link method was used to extrapolate the $P-S-N$ diagram to larger specimens. The extrapolated $P-S-N$ diagram was compared to experimental data. The effect of mean stress on fatigue strength of this material was also analyzed.

2. Experimental procedure

2.1. Material and specimens

The material under investigation was EN-GJS-400-18-LT ductile cast iron with graphite nodules contained within a ferritic matrix, Fig. 1. Tables 1 and 2 summarize the mechanical properties and chemical composition of the test material.

Specimens were taken from 750 mm \times 200 mm \times 95 mm cast blocks, Fig. 2. By changing the casting thickness and therefore cooling rate, the micro-structural properties of the ductile cast iron such as nodularity, nodule count and nodule size

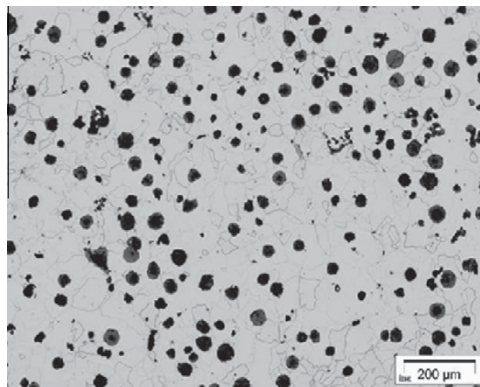


Fig. 1. Optical micrograph of the material.

Table 1
Mechanical properties.

0.2% Proof strength $R_{p0.2}$ (MPa)	Tensile strength R_m (MPa)	Reduction of area Z (%)	Modulus of elasticity E (GPa)
230	400	18	167

Table 2
Chemical composition wt.%, balance Fe.

C	Si	Mn	P	S	Ni	Mg
3.61	2.18	0.23	0.014	0.009	0.088	0.041

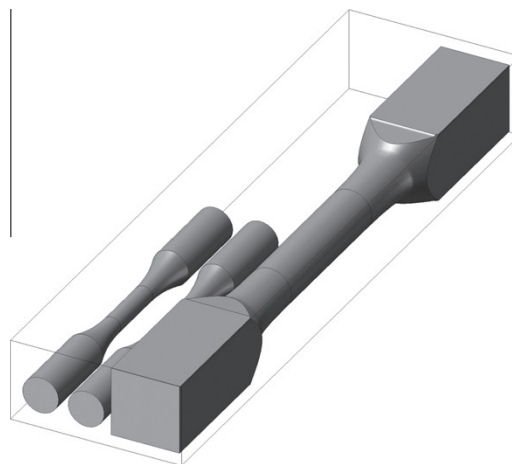


Fig. 2. Location of $\varnothing 21$ (left) and $\varnothing 50$ (right) specimens in the cast block.

change. These parameters have large influence on fatigue strength of baseline ductile cast iron. Thus, the thickness of the cast blocks in this research, Fig. 2, was selected to be representative of heavy-section castings for large wind turbines.

Two sets of specimens with diameters 21 mm and 50 mm were tested. Fig. 2 shows how specimens were taken out of the cast blocks. Detail drawings of the specimens are shown in Fig. 3. $\varnothing 21$ specimens were designed according to ASTM E 466 [17]. The recommended diameter by ASTM E 466 [17] for circular cross section specimens is maximum 25.4 mm. But heavy-section wind turbine cast components weight up to 24 tons. As noticed above, the fatigue strength of a material decreases with increasing specimen size. To evaluate geometrical size effect, and to obtain fatigue strength of large specimens representative of heavy-section wind turbine cast components, the second set of the specimens with 50 mm diameter, was designed. The specimens were designed to have the highest possible volume of material within the gage length relative to the volume of the complete specimen and to minimize the theoretical stress concentration factor, K_t of the specimens. Finite element simulations were performed to make sure that specimens will break in gage section.

One $\varnothing 21$ and one $\varnothing 50$ specimen was tested by 3D X-ray computed tomography [18] to find the potential defects within the material. No any defect larger than 0.2 mm was found in examined specimens. Thus, the only defects expected in the material are micro-shrinkages of size <0.2 mm.

2.2. Fatigue tests

Constant amplitude axial fatigue tests were conducted on cylindrical specimens in ambient air according to standard ASTM E 466 [17]. The specimens were cyclically loaded until failure by servo-hydraulic testing machine using a sinusoidal signal. Twelve $\varnothing 21$ specimens at load ratio of $R = 0$, twelve $\varnothing 21$ specimens at load ratio of $R = -1$ and twelve $\varnothing 50$ ones at load ratio of $R = -1$ were tested. $\varnothing 21$ and $\varnothing 50$ specimens were tested at 10 Hz and 1.0 Hz, respectively. Due to the large cross section of $\varnothing 50$ specimens and high loads used to test them, lower testing frequency was used for them. The testing frequency for $\varnothing 21$ and $\varnothing 50$ specimens was selected based on machine operator experience. Experimental set-up used to test $\varnothing 21$ and $\varnothing 50$ specimens is shown in Fig. 4a and b, respectively.

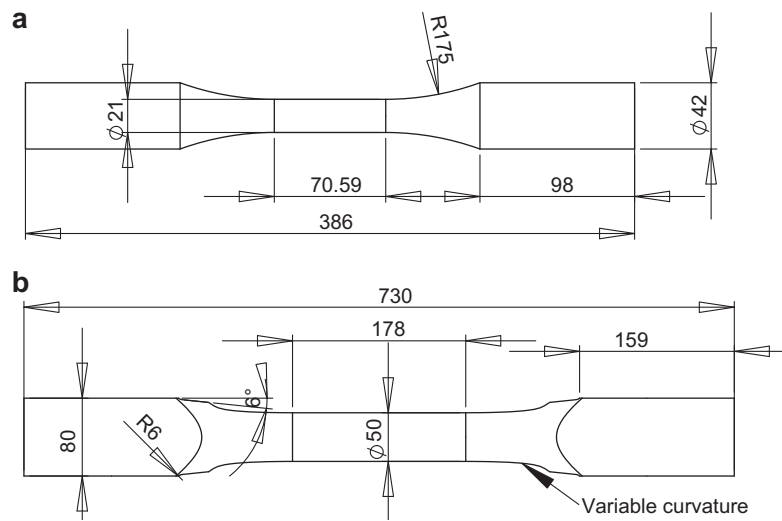


Fig. 3. Detail drawings of (a) Ø21 and (b) Ø50 specimens (all dimensions are in mm).

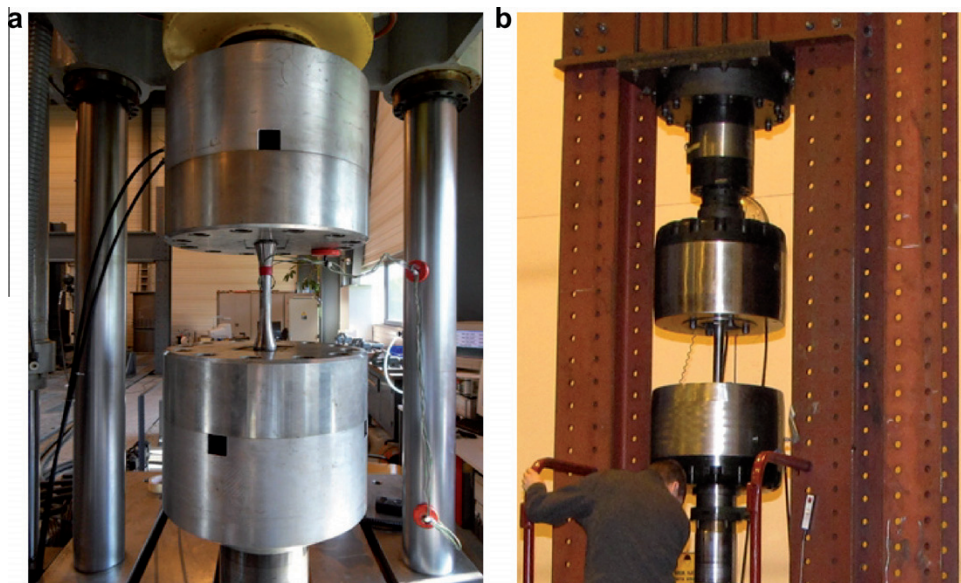


Fig. 4. Experimental set-up (a) Ø21 and (b) Ø50 specimens.

Different wind turbine cast components should endure 10 000 to several million cycles of fatigue life. The required range of endurances for the design purposes are 10,000–2 million cycles. The endurances for more than 2 million cycles can be estimated based on the obtained results for 10,000–2 million cycles. The stress levels adjusted to obtain the scatter of fatigue life between 10,000 and 2 million cycles. The stress levels are given in Appendix A. The specimens were investigated till final fracture in two parts, or up to at least 2 million cycles.

2.3. Fatigue test results

Fatigue test results are presented in Figs. 5 and 6, where the number of cycles to failure, N , has been plotted against the net section stress amplitude, σ_a . The registered value of N is for final fracture of specimen in two parts. Fig. 5 shows the comparison of fatigue strength for Ø21 and Ø50 specimens at $R = -1$. As should be expected, smaller specimens show a higher fatigue strength than larger specimens. Fig. 6 shows the comparison of fatigue strength for Ø21 specimens tested at load

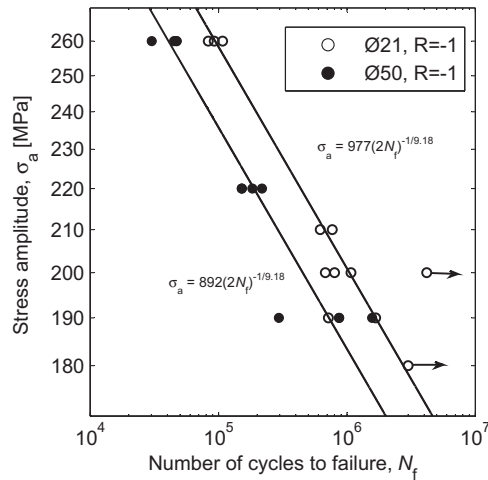


Fig. 5. Fatigue behaviour of EN-GJS-400-18-LT cylindrical specimens with different dimensions and load ratio $R = -1$.

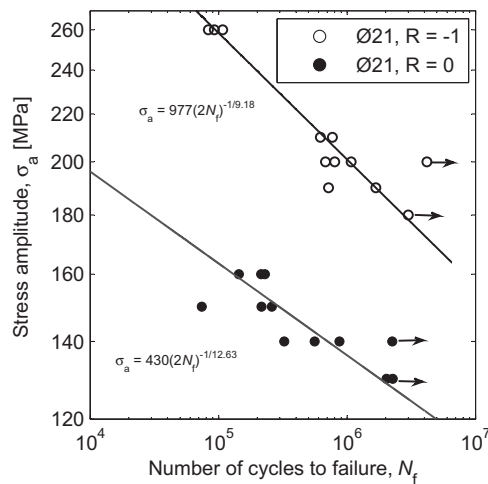


Fig. 6. Mean stress effect for $\varnothing 21$ specimens.

ratios of $R = 0$ and $R = -1$. Run out specimens are specified with an arrow. The test data have been tabulated in Appendix A, Tables 4–6.

The objective of this research was not to determine the fatigue limit of this material. As Fig. 5 shows, at stress amplitudes lower than 180 MPa, the material tends to have more than one million cycles of fatigue life. According to Ref. [19], the rotating bending fatigue limit for specimen with diameter of 10.5 mm made of baseline EN-GJS-400-18-LT is 195 MPa [20]. Usually rotating bending test results show higher strength than axial fatigue tests of the same specimens due to stress gradient over the rotating bending specimen cross section. There are two main factors which influence the fatigue strength of this material, geometrical and technological size effect. As shown in Fig. 5, larger specimens have lower fatigue strength than smaller ones (geometrical size effect) [21]. The fatigue strength of baseline ductile cast iron, changes by changing nodularity and nodule size. Thicker casting blocks have lower cooling rate and therefore material originated from thicker blocks has lower nodularity and nodule size [22,23]. This yields to a decrease in fatigue strength (technological size effect).

3. Statistical analysis of fatigue data

The goal of the statistical analysis is generally to find an $S-N$ curve at a probability level for which less than some small percentage of specimens would fail. If a large number of identical test pieces are run until fatigue failure, the number of

cycles sustained will differ from specimen to specimen. The probability of failure, P , has to be introduced and connected with the applied stress, σ , and the number of cycles to failure, N . These three parameters can be expressed in a P – S – N diagram. This contains a family of S – N curves, each curve corresponding to a particular value of the probability of failure, P . To establish such a P – S – N diagram, P – N relations at different stress levels should be experimentally determined. By having P – N relations, it will be possible to find, for every probability of failure, its related “number of cycles to failure” at different stress levels. Then for each particular probability of failure, the prescribed lives, N , at different stress levels should be connected to establish an S – N curve for the specified probability of failure. By repeating this process for different probabilities of failure, a family of S – N curves can be obtained [24]. This method requires a sufficient number of replications at each stress level. In this research just 12 specimens for each geometry at each load ratio have been tested. This number of data points was not enough to establish P – S – N curves based on P – N relations at different stress levels. Therefore an alternative method was used [25].

If it is assumed that the coefficient of variation in strength is constant, S – N curves for different probabilities of failure in a P – S – N diagram will be shifted by a constant amount in the S -direction. Therefore, if i data points are available, it is possible to pass i parallel S – N curves (on a log-log plot) through these data points and each S – N curve expresses one probability of failure, P . On the other hand, at each life, N , there will be i fatigue strength values. Such a diagram for $\varnothing 21$ specimens at $R = -1$ is shown in Fig. 7.

The question now arises of how to determine these parallel S – N curves. The S – N curve is often assumed to follow the Basquin equation

$$\sigma_a = \sigma'_f (2N_f)^{-\frac{1}{m}}, \quad (1)$$

where σ'_f is the fatigue strength coefficient and $-1/m$ the fatigue strength exponent. This curve will be a straight line on a log-log plot and may be found by linear regression analysis of fatigue data points.

3.1. Linear regression to find the Basquin exponent

Standard S – N diagrams found in most design texts are plotted with stress (independent variable) on the ordinate and number of cycles to failure (dependent variable) on the abscissa. The standard approach in curve fitting is to assume that the parameter plotted on the abscissa is the independent variable and that plotted on the ordinate is the dependent variable. But it should be noted that with fatigue data, stress is actually the independent variable and should be treated as such in the regression analysis. To treat cycles as the independent variable can lead to errors in the regression [26].

Taking the logarithm of Eq. (1) gives the following linear relationship:

$$\log(2N_f) = -m \log \sigma_a + m \log \sigma'_f, \quad (2)$$

or

$$y(x) = ax + b, \quad (3)$$

with $y = \log(2N_f)$, $x = \log \sigma_a$, $a = -m$, and $b = m \log \sigma'_f$. The standard least squares method can be used to find these constants for both $\varnothing 21$ and $\varnothing 50$ specimens. By increasing the number of data points, a better estimation of the average S – N curve can

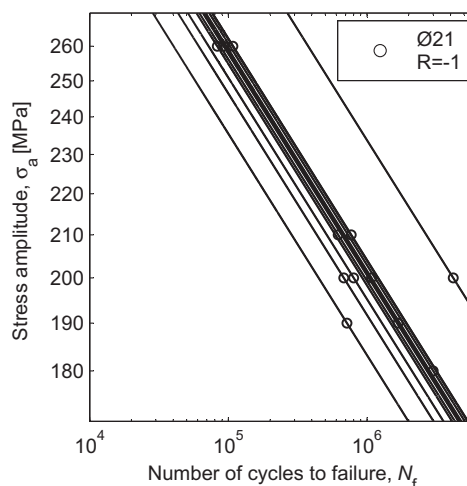


Fig. 7. A family of S – N curves passing through each data point for $\varnothing 21$ mm specimens, $R = -1$.

be obtained. In this research 12 data points per geometry at each load ratio are available. It is favorable to find a way to use all 24 data points at $R = -1$, instead of 12 data points, to determine $S-N$ curves.

According to weakest-link theory, $S-N$ curves for $\varnothing 21$ and $\varnothing 50$ specimens at $R = -1$ should be parallel. Therefore the $S-N$ curve for $\varnothing 21$ specimens has the form $y_1(x) = ax + b$ and for $\varnothing 50$ specimens $y_2(x) = ax + c$. By fulfilling the condition

$$\sum_{i=1}^k [y_i - y_1(x_i)]^2 + \sum_{j=1}^l [y_j - y_2(x_j)]^2 = \min, \quad (4)$$

it will be possible to use all 24 data points at $R = -1$ to find average $S-N$ curves. k and l are the total number of the data points available for $\varnothing 21$ and $\varnothing 50$ specimens at $R = -1$. Setting the partial derivatives of the left hand side, with respect to a , b , and c , equal to zero gives a system of linear equations to solve for a , b , and c

$$\begin{bmatrix} \sum_{i=1}^k x_i^2 + \sum_{j=1}^l x_j^2 & \sum_{i=1}^k x_i & \sum_{j=1}^l x_j \\ \sum_{i=1}^k x_i & k & 0 \\ \sum_{j=1}^l x_j & 0 & l \end{bmatrix} \begin{bmatrix} a \\ b \\ c \end{bmatrix} = \begin{bmatrix} \sum_{i=1}^k x_i y_i + \sum_{j=1}^l x_j y_j \\ \sum_{i=1}^k y_i \\ \sum_{j=1}^l y_j \end{bmatrix}. \quad (5)$$

By finding a , b , and c , it will be possible to establish the average $S-N$ curves. The obtained $S-N$ curves are presented in Fig. 5. One of the least square assumptions is that the dependent variable should be normal distributed. Except for substantial non-normality that leads to outliers in the $X-Y$ data, the linear regression statistic will not be much affected even if the population distributions are skewed.

To construct the family of $S-N$ curves shown in Fig. 7, first the average $S-N$ curve was drawn by means of the regression analysis of data and then the other curves were drawn parallel to the average $S-N$ curve.

It now becomes possible to evaluate the distribution of fatigue lives of specimens by regarding all of them as one set of data.

3.2. Weibull fatigue strength distribution

Weibull's weakest-link theory assumes a critical flaw to control failure. Thus, a stochastic distribution of flaws within specimens leads to scatter in the fatigue strength of the material. A weakest-link analysis can be formulated in two different ways, volume formulation and surface formulation [16,27]. In the volume formulation, the critical flaw is assumed to lie somewhere within the volume of the specimen. In the surface formulation, the controlling defects are assumed to be located at the surface of the specimen.

3.2.1. Volume formulation

In the volume formulation of the weakest-link theory [16], the probability of component failure P , can be expressed as

$$P_f = 1 - \exp \left[- \left(\frac{\bar{\sigma}_a}{\sigma_{A_0}(N)} \right)^{b_\sigma} \right]. \quad (6)$$

This equation describes a two-parameter Weibull distribution with shape and scale parameters b_σ and $\sigma_{A_0}^*(N)$. The Weibull stress amplitude $\bar{\sigma}_a$, which may also be referred to as the fatigue-effective stress amplitude, for volume formulation is defined as

$$\bar{\sigma}_a = \left(\frac{1}{V_0} \int_V \sigma_a^{b_\sigma} dV \right)^{\frac{1}{b_\sigma}}. \quad (7)$$

V_0 is an arbitrary reference volume, which may be thought of as the gage volume of the smooth fatigue specimens used to determine the $P-S-N$ data of the material. V is the component volume. The Weibull shape parameter b_σ , is a measure of the scatter of the fatigue strength and, indirectly, a measure of the scatter of the defect size distribution. b_σ increases with decreasing scatter in the fatigue strength.

3.2.2. Surface formulation

In the surface formulation of the weakest-link theory [16], the probability of component failure P , can be expressed as Eq. (6). The Weibull stress amplitude $\bar{\sigma}_a$ or the fatigue-effective stress amplitude, for surface formulation is now defined as

$$\bar{\sigma}_a = \left(\frac{1}{A_0} \int_A \sigma_a^{b_\sigma} dA \right)^{\frac{1}{b_\sigma}}. \quad (8)$$

A_0 is an arbitrary reference surface area, which may be thought of as the gage surface area of the smooth fatigue specimens used to determine the $P-S-N$ data of the material. A is the component surface area.

3.3. Weibull fatigue life distribution

In order to find $P-N$ relations at different stress levels, the Weibull fatigue life distribution is required. The Weibull fatigue strength distribution Eq. (6), can be transformed into a Weibull fatigue life distribution by using the Basquin equation Eq. (1). In the Weibull fatigue life distribution the probability of component failure P , can be expressed as

$$P_f = 1 - \exp \left[- \left(\frac{n}{N_0^m(\bar{\sigma}_a)} \right)^{b_n} \right], \tag{9}$$

where again b_n and $N_0^m(\bar{\sigma}_a)$ are Weibull shape and scale parameters. The Weibull exponent b_n is related to b_σ by

$$b_n = \frac{b_\sigma}{m}, \tag{10}$$

where $-1/m$ is the fatigue strength exponent in Basquin equation.

3.4. $P-S-N$ diagram

The Weibull fatigue life distribution, Eq. (9), was used to model the fatigue life for the specimens shown in Fig. 3. Since it was assumed that the $S-N$ curves for different probabilities of failure in a $P-S-N$ diagram at the same load ratio are parallel, the fatigue life distribution is the same at different stresses. Thus, it is sufficient to find fatigue life values for a single stress, σ_a , and fit Eq. (9) to these. By using Fig. 7 and fitting the Weibull distribution to the twelve fatigue lives at a single stress, $b_n = 3.41$ was obtained for $\varnothing 21$ specimens at $R = -1$. Using Eq. (10) one obtains $b_\sigma = 31.3$. The values of m to be used in Eq. (10) were given in Figs. 5 and 6. Using the same method, the values of b_n and b_σ for $\varnothing 50$ specimens at $R = -1$ are 3.03 and 27.82 and for $\varnothing 21$ specimens at $R = 0, 1.7$ and 21.47, respectively. To perform the statistical analysis, Minitab [28] was used and Weibull distribution parameters were obtained by least squares method. Run out specimens were treated as arbitrary censored data in the analysis performed by Minitab.

Finally, once the fatigue life distribution is known, it will be possible to establish a $P-S-N$ diagram. Fig. 8a and b shows the $P-S-N$ diagrams for $\varnothing 21$ specimens at $R = -1$ and $R = 0$. The $S-N$ curves for probabilities of failure of 10%, 50%, and 90% shown in Fig. 8 are in good agreement with the distribution of data points.

3.5. Size effect

As mentioned above, the fatigue strength of materials decreases with increasing component size. In most materials, fatigue initiates from material defects. By increasing the volume (or surface) of the component, the probability of failure increases due to the higher probability of finding a critical defect. Using Eqs. (6)–(8) the ratio between the fatigue strengths of axially loaded cylindrical specimens 1 and 2 becomes

$$\left(\frac{\sigma_{a2}}{\sigma_{a1}} \right) = \left(\frac{V_2}{V_1} \right)^{-\frac{1}{b_\sigma}}, \tag{11}$$

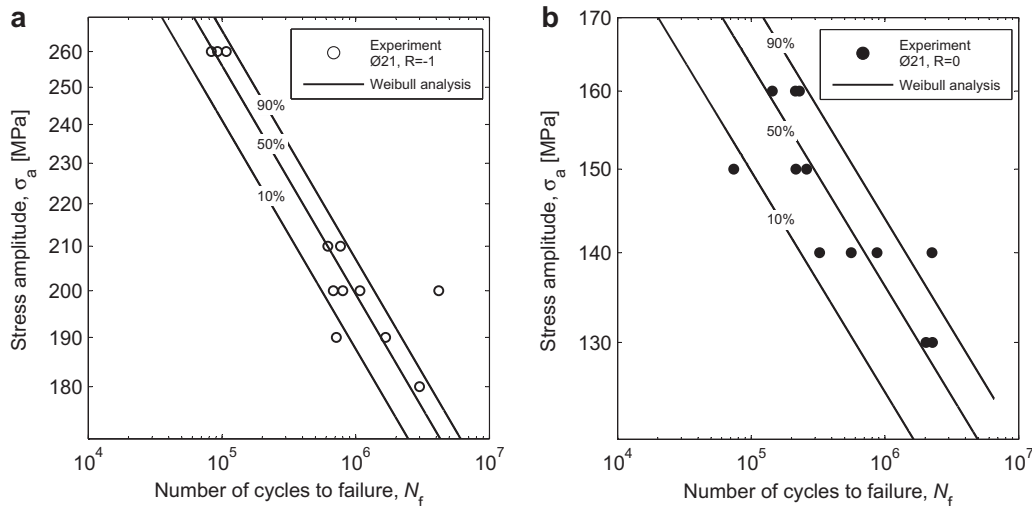


Fig. 8. $P-S-N$ diagrams for $\varnothing 21$ specimens at (a) $R = -1$ and (b) $R = 0$.

and

$$\left(\frac{\sigma_{a2}}{\sigma_{a1}}\right) = \left(\frac{A_2}{A_1}\right)^{\frac{1}{b\sigma}}, \quad (12)$$

respectively.

Generally Eqs. (7) and (8) should be calculated all over the component, in order to obtain the Weibull stress amplitude $\bar{\sigma}_a$. However, since in the current research the gage section of the fatigue specimens yields the dominating contribution to the stress integrals of Eqs. (7) and (8), their integrals were just calculated over the gage section of the fatigue specimens. Thus σ_a , V , and A , in Eqs. (11) and (12), are the nominal stress over the gage section, gage section volume and gage section surface area of fatigue specimens, respectively.

Both Eqs. (11) and (12) can be used to evaluate the effect of size on fatigue strength. Eq. (11) assumes the critical flaw to lie somewhere within the volume of the specimen (volume formulation) and Eq. (12) assumes the critical flaw to lie on the surface of the specimen (surface formulation).

As shown in Fig. 5, the fatigue properties for two sets of specimens have been obtained at $R = -1$. A first set of $\varnothing 21$ specimens have 4675 m² gage surface area and 24,450 m³ gage volume, a second set of $\varnothing 50$ specimens have 27,960 m² gage surface area and 349,500 m³ gage volume. Using Eqs. (11) or (12), it will be possible to extrapolate the $\varnothing 21$ P - S - N diagram shown in Fig. 8a to $\varnothing 50$ specimens at $R = -1$. Fig. 9 shows the comparison of the extrapolated $\varnothing 50$ P - S - N diagram obtained by the volume formulation, Eq. (11), with experimental data. Fig. 10 shows the comparison of the extrapolated $\varnothing 50$ P - S - N diagram obtained by the surface formulation, Eq. (12), with experimental data. The full lines show the extrapolated $\varnothing 50$ P - S - N diagram based on $\varnothing 21$ P - S - N diagram, the dotted lines the P - S - N diagram obtained by Weibull analysis of the original $\varnothing 50$ S - N data. In Fig. 9 both full line and dotted lines for probability of failure of 10% overlap each other. Table 3 compares the size factors, S_{a2}/S_{a1} , predicted by Eqs. (11) and (12) based on $\varnothing 21$ specimens at $R = -1$, with experimental results.

In this research, failure initiates from the surface in all specimens, but, as can be seen from the Figs. 9 and 10 and Table 3, the volume formulation yields a better prediction than surface formulation. The distribution of data points is well described by means of the extrapolated S - N curves obtained by volume formulation of Weibull's weakest-link theory.

3.6. Normalized fatigue life distribution

As shown in Fig. 2, both $\varnothing 21$ and $\varnothing 50$ specimens were taken from the same set of cast blocks and therefore belong to the same population. As mentioned above, since there were not enough replications to determine P - N relations at each stress level, an alternative method was used to establish a P - S - N diagram. Without copious replications, the data can again be condensed by using the normalized fatigue life X_i , of all 24 specimens tested at $R = -1$ to find Weibull distribution parameters.

Let a specimen have a life N_i at σ_{ai} . The normalized fatigue life is

$$X_i = \frac{N_i}{N_f(\sigma_{ai})}, \quad (13)$$

where $N_f(\sigma_{ai})$ is the estimated average fatigue life at stress amplitude of σ_{ai} , and may be obtained by the Basquin equations presented in Fig. 5.

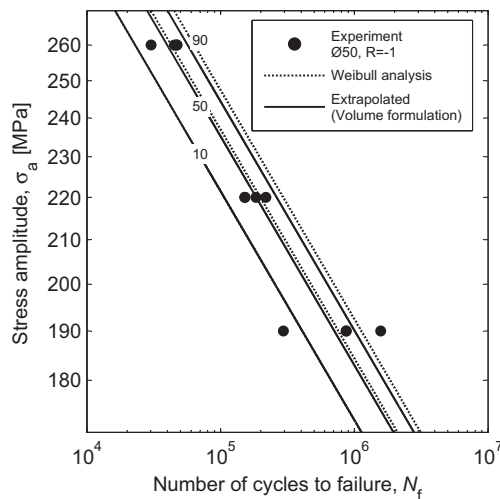


Fig. 9. Comparison of extrapolated P - S - N diagram for $\varnothing 50$ specimens obtained by volume formulation with experimental data, $R = -1$.

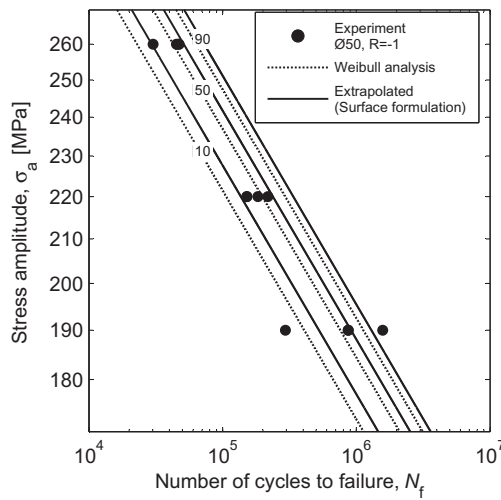


Fig. 10. Comparison of extrapolated P - S - N diagram for $\varnothing 50$ specimens obtained by surface formulation with experimental data, $R = -1$.

Table 3

Comparison of the size factor predicted by Weakest-link method based on $\varnothing 21$ specimens with experimental results, $R = -1$.

Size factor	$\frac{S_{a\varnothing 50}}{S_{a\varnothing 21}}$
Experiment	0.913
Volume formulation	0.919
Surface formulation	0.944

If it is assumed that the coefficient of variation of the fatigue life, N , is constant, the normalized fatigue life can be considered as a statistical variable reflecting the fatigue life distribution of the material.

Fig. 11 shows the Weibull plot for the normalized fatigue lives of the $\varnothing 21$ and $\varnothing 50$ specimens tested at $R = -1$. The Weibull shape parameter for this merged normalized fatigue lives becomes $b_n = 3.26$ and, by using Eq. (10), $b_\sigma = 29.93$.

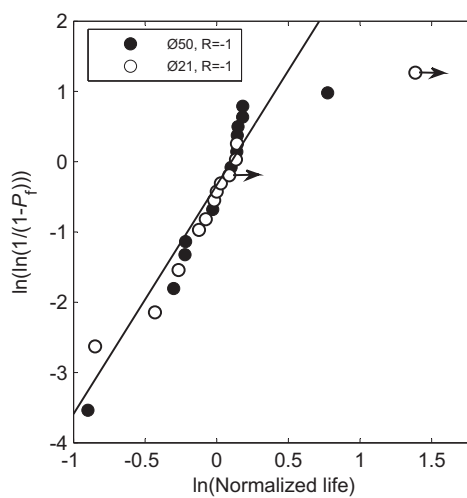


Fig. 11. Weibull plot of normalized fatigue lives.

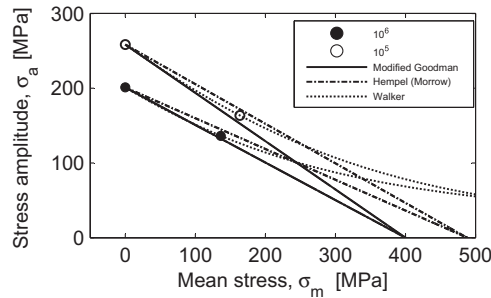


Fig. 12. Relationship between stress amplitude, σ_a , and mean stress, σ_m , for EN-GJS-400-18-LT.

4. Mean stress effect

Clearly, service stress cycles are not always fully reversed. The empirical modified Goodman [29], Hempel [30] (Morrow [31]) and Walker [32] approaches may be used to quantify the effect of mean stress on the fatigue strength. The required material parameters for the Hempel and Walker approaches, may be deduced from the mean stress sensitivity

$$M = \frac{\sigma_a(R = -1)}{\sigma_a(R = 0)} - 1, \quad (14)$$

a parameter introduced by Schütz [33]. σ_a denotes the fatigue strength at a given stress ratio and number of cycles. Based on fatigue tests on EN-GJS-400-15, Kaufmann [34] suggested $M = 0.3$ to be used for 'defect-free' material and $M = 0.5$ for material with defects such as dross, chunky graphite and pipe. In the present study, the material is 'defect-free' and $M = 0.48$ is obtained for 10^6 cycles.

According to the modified Goodman approach

$$\frac{\sigma_a}{\sigma_{ar}} + \frac{\sigma_m}{R_m} = 1, \quad (15)$$

where σ_{ar} , σ_m , and R_m are the fatigue strength at zero mean stress, mean stress and tensile strength of the material, respectively. Since the modified Goodman equation is usually conservative at tensile mean stresses, Hempel suggested to modify it by replacing R_m with true fracture strength R'_m

$$R'_m = \frac{R_m}{1 - Z}, \quad (16)$$

where Z is area reduction after fracture in a tensile test. With data from Table 1, R'_m becomes 488 MPa.

The Walker equation can be expressed as

$$\bar{\sigma}_{ar} = \sigma_{\max} \left(\frac{1 - R}{2} \right)^\gamma. \quad (17)$$

For $\varnothing 21$ specimens, the stress amplitude, σ_a , corresponding to 50% failure probability has been plotted against mean stress, σ_m , in Fig. 12 for 10^5 and 10^6 cycles at $R = 0$ and $R = -1$. The Walker equation was fitted to the points represented in Fig. 12. The obtained Walker exponents for 10^5 and 10^6 cycles are $\gamma = 0.34$ and $\gamma = 0.44$, respectively.

The Modified Goodman, Hempel and Walker equations have been plotted in Fig. 12 for the material tested in this research.

5. Conclusion

Fatigue tests were conducted on cylindrical specimens at load ratios of $R = 0$ and $R = -1$. Experiments were carried out on two sets of specimens with different dimensions. The material under investigation was EN-GJS-400-18-LT ductile cast iron for wind turbine use. Statistical analysis of fatigue data was done by means of the two-parameter Weibull distribution. Mean stress effect was evaluated.

- Fatigue properties of EN-GJS-400-18-LT ductile cast iron was presented.
- The geometrical size effect on fatigue strength of EN-GJS-400-18-LT ductile cast iron was experimentally evaluated.
- The mean stress effect was experimentally evaluated.
- P - S - N diagrams for EN-GJS-400-18-LT ductile cast iron were determined by means of the Weibull distribution.
- The obtained P - S - N diagrams expressed the distribution of data points well.

- Weibull's weakest-link method was used to predict the P – S – N diagram for larger specimens based on the P – S – N diagram for smaller specimens.
- Comparison with experimental results showed that the predicted P – S – N diagram for larger specimens can successfully represent the distribution of data points.
- It was found that in this research, the volume formulation of Weibull's weakest-link method yields a better extrapolation of the P – S – N diagram for larger specimens than the surface formulation.

Acknowledgments

The authors would like to acknowledge financial and technical support by FeVIND, a project under the auspices of the Research Council of Norway. In particular, thanks are due to Vestas Wind Systems AS for providing the cast material and supporting the fatigue testing. The fatigue tests were carried out to our full satisfaction by Marintek, Trondheim ($\varnothing 50$ specimens) and IEHK, RWTH, Aachen ($\varnothing 21$ specimens).

Appendix A. 21 and 50 specimens fatigue test data

Table 4

$\varnothing 21$ specimen fatigue test data, load ratio $R = -1$.

Specimen number	Stress amplitude (MPa)	Fatigue life	Comment
1	180	3,000,000	Run out
2	190	716,400	Broken
3	190	1,674,100	Broken
4	200	679,400	Broken
5	200	801,000	Broken
6	200	1,076,600	Broken
7	200	4,181,701	Run out
8	210	619,200	Broken
9	210	769,500	Broken
10	260	83,200	Broken
11	260	92,500	Broken
12	260	107,700	Broken

Table 5

$\varnothing 50$ specimen fatigue test data, load ratio $R = -1$.

Specimen number	Stress amplitude (MPa)	Fatigue life	Comment
1	190	295,000	Broken
2	190	869,000	Broken
3	190	869,900	Broken
4	190	1,573,335	Broken
5	220	151,400	Broken
6	220	152,000	Broken
7	220	183,700	Broken
8	220	218,000	Broken
9	260	30,200	Broken
10	260	45,100	Broken
11	260	46,900	Broken
12	260	47,300	Broken

Table 6

$\varnothing 21$ specimen fatigue test data, load ratio $R = 0$.

Specimen number	Stress amplitude (MPa)	Stress amplitude (MPa)	Fatigue life	Comment
1	130	130	2,028,248	Broken
2	130	130	2,268,764	Run out
3	140	140	324,321	Broken
4	140	140	559,564	Broken
5	140	140	873,310	Broken
6	140	140	2,249,246	Run out
7	150	150	74,003	Broken
8	150	150	215,864	Broken
9	150	150	259,504	Broken
10	160	160	143,683	Broken
11	160	160	214,158	Broken
12	160	160	229,307	Broken

References

- [1] Roedter H, Gagne M. Ductile iron for heavy section wind mill castings: a European experience. In: Keith Millis symposium on ductile cast iron, 2003.
- [2] EN 12680-3:2003. Founding – ultrasonic examination. Part 3: Spheroidal graphite cast iron castings. CEN; August 2003.
- [3] EN 1369:1997. Founding – magnetic particle inspection. CEN; July 1997.
- [4] Lloyd Germanischer. Guideline for the certification of offshore wind turbines. Hamburg Germany; 2005.
- [5] Nadot Y, Mendez N, Ranganathan N, Beranger A. Fatigue life assessment of nodular cast iron containing casting defects. *Fatigue Fract Eng Mater Struct* 1999;22(4):289–300.
- [6] Wang Q, Bathias C. Fatigue characterization of a spheroidal graphite cast iron under ultrasonic loading. *J Mater Sci* 2004;39(2):687–9.
- [7] Sonsino C, Zinke R, Heinrietz A, Heim R, Hanselka H, Streicher M. Structural durability criteria for commercial vehicle components from the self strengthening cast ausferrite nodular iron EN-GJS-800-8 (ADI) in comparison to the ferritic EN-GJS-400-15. *Materialwiss Werkst* 2008;39(10):761–8.
- [8] Xue H, Bayraktar E, Bathias C. Damage mechanism of a nodular cast iron under the very high cycle fatigue regime. *J Mater Process Technol* 2008;202(1–3):216–23.
- [9] Lampman S et al. *ASM Handbook. Fatigue Fract*, ASM Int 1996;19:741.
- [10] Phillips C, Heywood R. The size effect in fatigue of plain and notched steel specimens loaded under reversed direct stress. *Proc Inst Mech Eng* 1951;165:113–24.
- [11] Gaenser H. Some notes on gradient, volumetric and weakest link concepts in fatigue. *Comput Mater Sci* 2008;44(2):230–9.
- [12] Carpinteri A, Spagnoli A, Vantadori S. Size effect in $S-N$ curves: a fractal approach to finite-life fatigue strength. *Int J Fatigue* 2009;31(5):927–33.
- [13] Weibull W. A statistical theory of the strength of materials. *Ingeniörsvetenskapsakademiens handlingar*, vol. 151. Stockholm: Generalstabens Litograska Anstalts Förlag; 1939. p. 145.
- [14] Weibull W. The phenomenon of rupture in solids. *Ingeniörsvetenskapsakademiens handlingar*, vol. 153. Stockholm: Generalstabens Litograska Anstalts Förlag; 1939. p. 155.
- [15] Weibull W. A statistical distribution function of wide applicability. *J Appl Mech* 1951;18(3):293–7.
- [16] Wormsen A, Sjödin B, Härkegård G, Fjeldstad A. Non-local stress approach for fatigue assessment based on weakest-link theory and statistics of extremes. *Fatigue Fract Eng Mater Struct* 2007;30(12):1214–27.
- [17] ASTM Standard E 466-07. Standard practice for conducting force controlled constant amplitude axial fatigue tests of metallic materials. West Conshohocken (PA, USA): ASTM International; 2007.
- [18] Shirani M, Härkegård G. Fatigue crack growth simulation in components with random defects. *J ASTM Int* 2009;6(9).
- [19] EN 1563:1997. European standard, Founding – spheroidal graphite cast irons. CEN; June 1997.
- [20] Palmer KB, Gilbert GNJ. BCIRA research report 361. *J Res Develop* 1953;5(1):2–14.
- [21] Shirani M, Härkegård G, Morin N. Fatigue life prediction of components made of spheroidal graphite cast iron. *Proc Eng* 2010;2(1):1125–30.
- [22] Ru G, Doshi B. Relationship between mechanical properties and graphite structure in cast irons. II. Ductile iron. *Mod Cast* 1980;70(7):70–4.
- [23] Lin CK, Wei JY. High-cycle fatigue of austempered ductile irons in various-sized Y-block castings. *Mater Trans JIM* 1997;38(8):682–91.
- [24] Weibull W. *Fatigue testing and analysis of results*. New York: Pergamon; 1961.
- [25] Nishijima S. Statistical fatigue properties of some heat-treated steels for machine structural use. *ASTM Spec Technol Publ* 1981(744):75–88.
- [26] Wilson J. Statistical comparison of fatigue data. *J Mater Sci Lett* 1988;7(3):307–8.
- [27] Belmonte H, Mulheron M, Smith P. Weibull analysis, extrapolations and implications for condition assessment of cast iron water mains. *Fatigue Fract Eng Mater Struct* 2007;30(10):964–90.
- [28] Inc M. Minitab, release 15 for windows. State College (PA): Minitab Inc; 2007.
- [29] Smith J. The effect of range of stress on the fatigue strength of metals. *Univ Illinois Eng Exp Sta, Bull* 1942;334(26):39.
- [30] Hempel M. Das Dauerschwingverhalten der Werkstoffe. *VDI-Z* 1962;104:1362–77.
- [31] Morrow J. *Fatigue design handbook*. Adv Eng 1968;4(3.2):21–9.
- [32] Walker K. The effect of stress ratio during crack propagation and fatigue for 2024-T3 and 7075-T6 aluminum. In: *Effects of environment and complex load history on fatigue life: a symposium presented at the Fall Meeting of the American Society for Testing and Materials, Atlanta, Ga., 29 September–4 October, 1968*, ASTM International; 1970. p. 1.
- [33] Schütz W. Über eine beziehung zwischen der lebensdauer bei konstanter und bei veränderlicher beanspruchungsamplitude und ihre anwendbarkeit auf die bemessung von flugzeugbauteilen. *Z Flugwissensch* 1967;15:407–19.
- [34] Kaufmann H, Wolters D. Zyklische beanspruchbarkeit dickwandiger bauteile aus ferritischem gueisen mit kugelgraphit. *Konstruieren Giessen* 2002;27(1):427.

Paper 2

Large scale axial fatigue testing of ductile cast iron for heavy section wind turbine components

M. Shirani^{a,*}, G. Härkegård^a

^aNorwegian University of Science and Technology, Dept. of Engineering Design and Materials, NO-7491 Trondheim, Norway

Abstract

The present paper deals with axial fatigue testing of heavy section EN-GJS-400-18-LT ductile cast iron specimens with 120 mm × 140 mm cross section and also smaller cylindrical specimens with 21 mm diameter at room temperature and load ratio $R = -1$. The load levels for heavy section specimens were adjusted to cover endurance from 10 000 to 14 million cycles. Each heavy section specimen weights 380 kg. The specimens were cut from castings with 150 mm thickness. The heavy section specimens thickness is close to the common thicknesses of heavy section wind turbine ductile cast iron components. Fatigue strength of large 120 mm × 140 mm specimens were compared with fatigue strength of smaller 21 mm diameter specimens and geometrical size effect was evaluated. To evaluate the wall thickness effect on fatigue strength (technological size effect), the obtained fatigue test results for 21 mm specimens from billets with 150 mm thickness were compared with the published fatigue test results of the same specimens but from billets with 95 mm thickness. Metallography analysis of 21 mm specimens from billets with 95 mm and 150 mm thicknesses were performed and important microstructural parameters were measured and compared. Finally the effect of casting thickness and microstructure on fatigue strength of this material was evaluated.

Keywords: Heavy section component, large scale axial fatigue testing, geometrical size effect, technological size effect, EN-GJS-400-18-LT

1. Introduction

Wind turbine manufacturers have to compete with other sources of energy such as natural gas and coal. In order to produce cheaper wind electricity, larger and lighter wind turbines have to be developed. Cast components make up much of the weight of the wind turbine. The majority of wind turbine parts are made out of the challenging ductile iron grade EN – GJS – 400 – 18 – LT [1].

The current design of heavy section wind turbine cast components is based on safe life design philosophy [2]. In the safe life design, $S - N$ curves are derived from fatigue testing on baseline material. To implement these $S - N$ curves in design of a real component, large reduction factors must be used to account for different parameters. Thus, to develop larger, lighter and more powerful wind turbines, good knowledge of fatigue behavior of EN-GJS-400-18-LT is required.

*Corresponding author. Tel.: +47 735 93761; fax: +47 735 94129.
Email address: mehdi.shirani@ntnu.no (M. Shirani)

It is a well known phenomenon that the fatigue strength of a material decreases with increasing specimen size (size effect) [3-5]. Specimens with different sizes but from castings with the same cooling rate, show different fatigue strength (geometrical size effect) [6]. Also, specimens with the same geometry, but from the castings with different cooling rates show different fatigue strength (technological size effect).

To apply the experimentally obtained $S - N$ curves in fatigue design of heavy section wind turbine cast iron components, both geometrical and technological size effect should be considered. But there is no robust methodology to apply the appropriate factors to $S - N$ curves to take into account both geometrical and technological size effect. Therefore, large reduction factors are usually applied to $S - N$ curves based on laboratory-size specimens to take into account size effect. This yields over design of these components. To counter this problem and eliminate uncertainties in fatigue design of large wind turbine cast iron components, it is recommended to perform fatigue testing on fatigue specimens with the dimensions and thicknesses close to heavy section wind turbine cast iron components [2]. To the best of the authors' knowledge, almost all $S - N$ curves published on fatigue behavior of EN-GJS-400-18-LT are limited to small laboratory-size tested specimens [6-8].

In this research, fatigue specimens with 120 mm \times 140 mm cross section were designed to establish $S - N$ curves for heavy section wind turbine components. Specimens were cut from 150 mm \times 300 mm \times 1550 mm EN-GJS-400-18-LT blocks.

To evaluate geometrical size effect, besides the first set of heavy section 120 mm \times 140 mm specimens, the second set of specimens with 21 mm diameter were axially fatigue tested at load ratio $R = -1$. The specimens were cut from 150 mm \times 300 mm \times 1550 mm EN-GJS-400-18-LT blocks.

Statistical analysis of the fatigue strength of the specimens was done using the Weibull distribution [9-12], and $P - S - N$ diagrams were established. Weakest link method was used to model the geometrical size effect and predict the $S - N$ curves for heavy section 120 mm \times 140 mm specimens, based on fatigue test results of $\varnothing 21$ specimens.

The morphology of the graphite in cast iron significantly influences the mechanical properties [13-16]. By increasing the casting thickness, the cooling rate decreases and the nodularity and nodule count of the microstructure decreases. This yields a decrease in fatigue strength (technological size effect). To evaluate the casting thickness effect (technological size effect) on fatigue strength of the analyzed material, the fatigue test results obtained for $\varnothing 21$ specimens in this research are compared to the published results in Ref. [6] for the same fatigue specimens but with different cooling rate. The $\varnothing 21$ specimens tested in this research were from cast blocks with 150 mm thickness. The $\varnothing 21$ specimens tested in Ref. [6] have the same geometry and dimensions, but were from cast billets with 95 mm thickness.

To evaluate the effect of casting thickness (cooling rate) on microstructure and the effect of microstructure on fatigue strength, metallography of twelve $\varnothing 21$ specimens from cast blocks with 95 mm and 150 mm thickness were performed and important micro structural parameters were measured and compared.

2. Experimental procedure

2.1. Material

The material under investigation was EN - GJS - 400 - 18 - LT ductile cast iron with graphite nodules contained within a ferritic matrix, Fig. 1a.

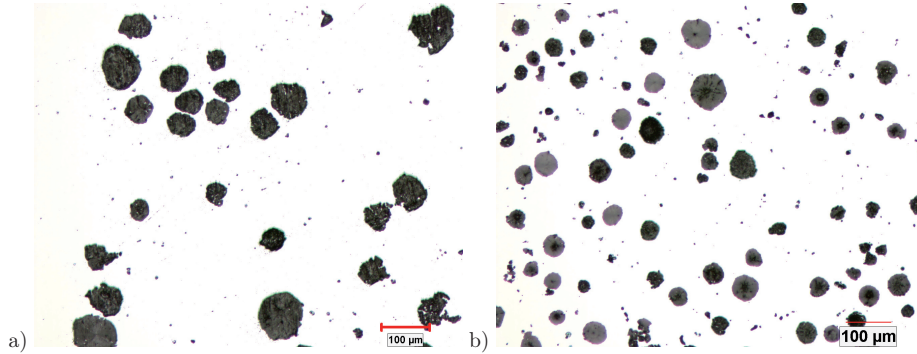


Figure 1: Representative optical micrograph of the EN-GJS-400-18-LT test material a) cast blocks with 150 mm thickness b) cast blocks with 95 mm thickness [6].

Specimens were taken from 150mm × 300mm × 1550mm cast blocks. Tensile tests were performed on 10 tensile specimens cut from core and rim zone areas of the cast block [17]. Specimens number 1, 3, 4, 6, 7 and 9 were from rim zone and specimens 2, 5, 8 and 10 were from core zone. Table 1 summarizes tensile test results for the 10 tested specimens. Based on the data presented in Table 1, no conclusion could be made on the effect of the specimens position in initial block on 0.2 % proof strength, tensile strength, reduction of area and elongation of the examined specimens. Table 2 summarizes the chemical composition of the test material.

According to EN- 1563: 1997 [7], 0.2 % proof strength, tensile strength and elongation of EN-GJS-400-18-LT casting with 150 mm thickness are 220 MPa, 370 MPa and 12%. Among the 10 tested specimens, just specimens number 3 and 9 have elongation close to the standard for 150 mm thick EN-GJS-400-18-LT block. Specimen number 10 shows very low elongation and tensile strength. This specimen was from the core zone of the cast block.

2.2. Specimens

Two sets of specimens were machined. The first set of specimens with 21 mm diameter ($\varnothing 21$) and the second set of heavy section specimens with 120 mm × 140 mm cross section. The dimensions of the initial cast blocks were 150 mm × 300 mm × 1550 mm. One heavy section specimen was machined out of each block. Detail drawings of the specimens are shown in Fig. 2.

$\varnothing 21$ specimens were designed according to ASTM E 466 [18]. The heavy section 120 mm × 140 mm specimens were designed to have the highest possible volume of material tested per specimen

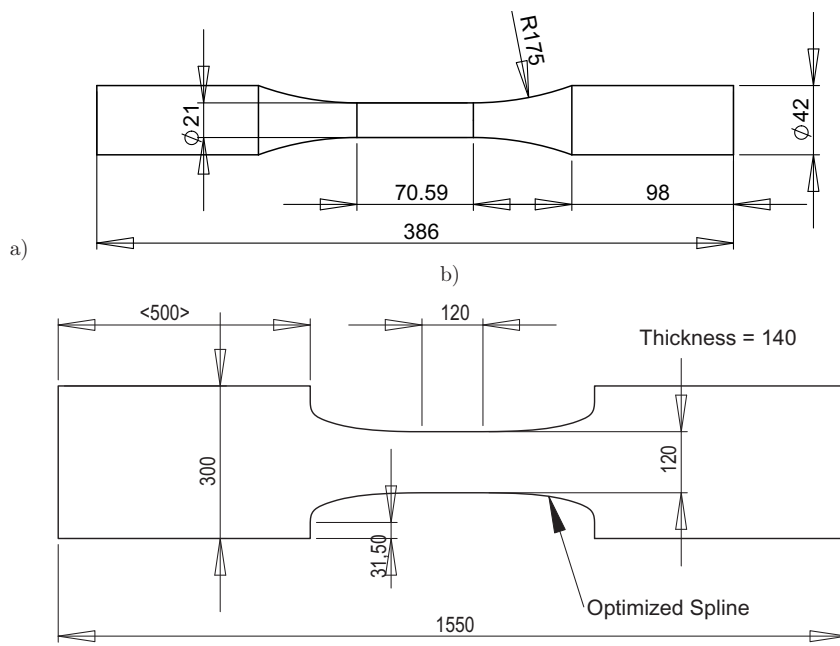


Figure 2: Detail drawings of (a) $\varnothing 21$ and (b) $120 \text{ mm} \times 140 \text{ mm}$ specimens (all dimensions are in mm).

Table 1: Mechanical properties.

Specimen number	0.2 % proof strength $R_{p0.2}$ (MPa)	Tensile strength R_m (MPa)	Reduction of area Z (%)	Elongation at fracture A_5 (%)	Uniform elongation A_g (%)	Zone
1	241	318	5.44	4.7	4.53	Rim
3	241	349	12.66	10.2	9.15	Rim
4	240	312	6.12	5.4	4.43	Rim
6	241	324	7.86	5.3	5.12	Rim
7	239	319	8.56	5.4	5.08	Rim
9	240	354	13.81	13.3	11.75	Rim
2	240	326	6.64	6.2	5.53	Core
5	239	323	7.50	6	5.38	Core
8	238	324	6.76	5.7	5.36	Core
10	238	296	5.57	2.5	2.3	Core

Table 2: Chemical composition wt.%, balance Fe.

C	Si	Mn	P	S	Ni	Mg
3.61	2.18	0.23	0.014	0.009	0.088	0.041

relative to the volume of the complete specimen and the lowest possible stress concentration in the transition area from clamp section to gage section and to prevent failure in the clamp section.

Fig. 3 shows the initial design sketch for heavy section fatigue specimens. The fatigue machine clamp diameter was 500 mm, so the length of the specimen head could not be less than 500 mm. The total length of the specimens was equal to the total length of the initial cast blocks, 1550 mm. The unknown parameters were gage section length, L_g and gage section width, W . Moreover, a variable curve should connect clamp section to the gage section.

According to experience, there is a probability that the fatigue specimen fails in the clamp area rather than the gage section. Specified area in Fig. 4b shows the critical area for fatigue failure in the clamp section. Finite element simulations showed that in order to keep maximum principal stress in the specified critical area in Fig. 4b, about 20% lower than the gage section and prevent component failure in the clamp section, the gage section width should not be greater than 120 mm. Thus, the gage section width was fixed to 120 mm. In initial calculations, the variable curve which connects clamp section to the gage section was considered to be a circular curve and the clamp section was connected to the gage section with a circular curve with 302 mm radius.

Fig. 4a shows the representative maximum principal stress distribution over the initially designed fatigue specimen surface. The stress concentration in the transitional area from clamp section to the gage section is $K_t = 1.11$. This increases the probability of failure in the transitional area in comparison with the gage section.

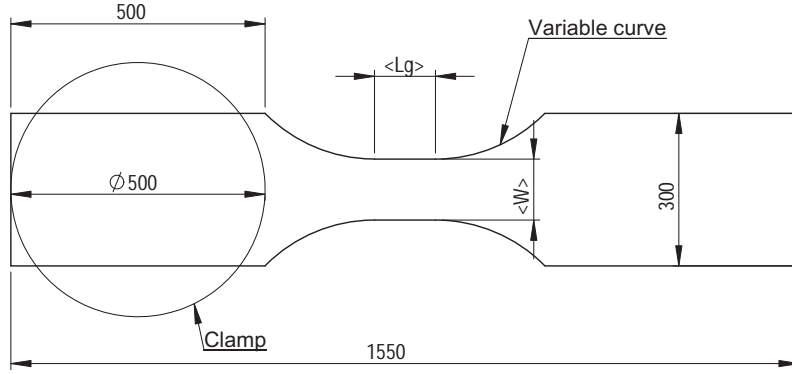


Figure 3: Initial design sketch for the heavy section fatigue specimens (all dimensions are in mm).

The blue area in Fig. 5a shows the volume of the material which is subjected to 90% of the peak value of maximum principal stress in axial fatigue testing. As can be seen, a relatively small volume of the material is tested in this initial design.

To counter these problems, shape optimization was performed on the transitional curve from clamp section to gage section, to minimize the theoretical stress concentration factor, K_t , of the specimens and increase the volume of the material which is tested per specimen. The shape optimization was performed by ANSYS. Fig. 2b shows the dimensions of the optimized final heavy section specimens. Fig. 4b shows maximum principal stress distribution over the optimized final heavy section specimen surface. Fig. 5b shows the volume of the material which is subjected to 90% of the peak value of the maximum principal stress in the final optimized design.

Finally the stress concentration in the transition area of the heavy section specimens was reduced from $K_t = 1.11$ in initial design to $K_t = 1.04$ in the final optimized design. Fig. 6b shows the comparison of maximum principal stress distribution over the specified path in Fig. 6a for initial design and final optimized design.

2.3. Fatigue tests

2.3.1. $\varnothing 21$ specimens

Constant amplitude axial fatigue tests were conducted on cylindrical $\varnothing 21$ specimens in ambient air according to standard ASTM E 466 [18]. The specimens were cyclically loaded until failure by

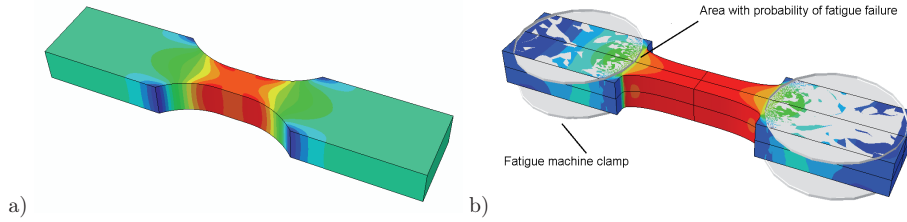


Figure 4: Representative maximum principal stress distribution over the fatigue specimen surface a) initially designed specimen with circular transitional curve b) final specimen with optimized transitional curve.

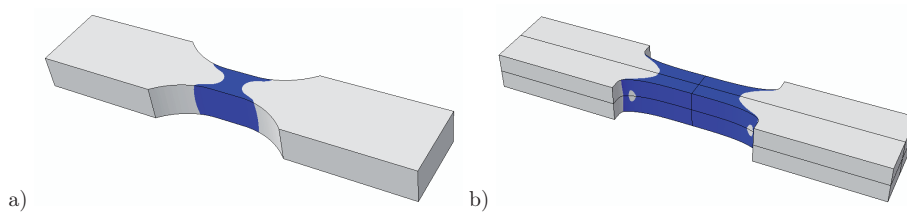


Figure 5: Blue area shows the volume of the material which is subjected to 90% of the peak value of maximum principal stress in axial fatigue testing a) initial design b) final optimized design.

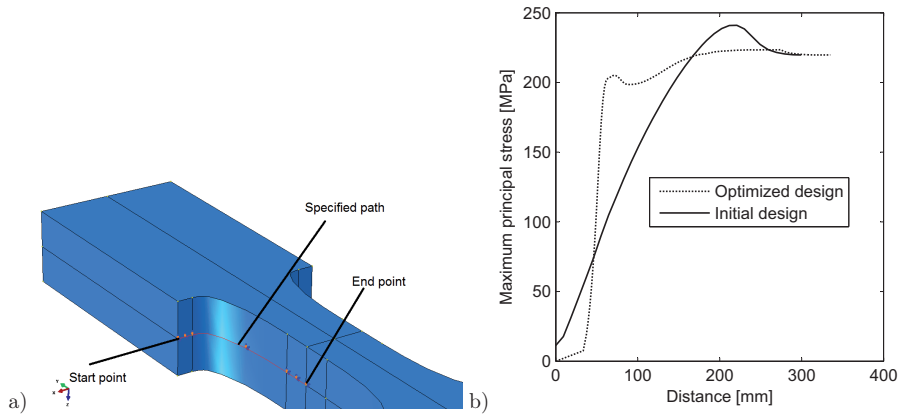


Figure 6: a) Specified path over the transitional area and gage section of the specimens b) comparison of the maximum principal stress distribution over the specified path for initial and optimized designs.



Figure 7: Experimental set-up for fatigue testing of $\varnothing 21$ specimens.

servo-hydraulic testing machine using a sinusoidal signal. Eighteen $\varnothing 21$ specimens at load ratio of $R = -1$ were tested. The specimens were tested at 10 Hz. The testing frequency for $\varnothing 21$ was selected based on machine operator experience. Experimental set-up used to test $\varnothing 21$ specimens is shown in Fig. 7. To make sure that the specimens have been aligned correctly and the bending stress is within the acceptable range, four strain gages were attached to each specimen and the strains were registered at four positions along the perimeter.

The stress levels for $\varnothing 21$ specimens were chosen to obtain fatigue lives (to fracture) between 10,000 and 2.5 million cycles. The stress levels are given in Appendix A.

2.3.2. Heavy section $120\text{ mm} \times 140\text{ mm}$ specimens

Constant amplitude axial fatigue tests were conducted on $120\text{ mm} \times 140\text{ mm}$ heavy section specimens in ambient air. The specimens were cyclically loaded until failure by a 12 MN resonance testing machine at a frequency of about 40 Hz. The diameter of clamping device is 500 mm and the



Figure 8: Experimental set-up for fatigue testing of 120 mm × 140 mm specimens.

clamping force was 10 MN. Nine heavy section specimens were tested at a load ratio of $R = -1$. The experimental set-up used to test 120 mm × 140 mm specimens is shown in Fig. 8. To make sure that the specimens have been correctly aligned, four strain gages were attached to each specimen and the strains were registered at four positions along the perimeter. Fig. 9 shows the cross section of a broken 120 mm × 140 mm specimen. As can be seen, fatigue cracks initiate from two opposite sides of the specimen. The nearly symmetric fatigue crack propagation indicates that the bending stresses were small.

A thermocouple was attached to the test specimen. At the beginning of the fatigue test, the specimen temperature increased rapidly and then stabilized at around 100°C.

In order to be able to use the obtained test results for heavy section specimens in future design of heavy section wind turbine cast iron components, the entire test procedure, from specimen design to fatigue testing was certified by Germanischer Lloyd Industrial Services.



Figure 9: Cross section of a broken 120 mm \times 140 mm specimen.

Different wind turbine cast components usually should endure 10 000 to 14 million cycles of fatigue life. Almost all available endurance data on fatigue strength of EN-GJS-400-18-LT is up to 2 million cycles [6]. For design purposes, the endurance for more than 2 million cycles can be estimated based on the obtained results for 10 000 - 2 million cycles. This may yield an over-design of the components. In order to solve this problem, the stress levels for heavy section specimens were chosen to obtain fatigue lives (to fracture) between 10 000 and 14 million cycles. The stress levels are given in Appendix A.

2.4. Fatigue test results

Fatigue test results are presented in Fig. 10, where the number of cycles to fracture, N_f , has been plotted against the net section stress amplitude, σ_a . Fig. 10 shows the comparison of fatigue strength for $\varnothing 21$ and 120 mm \times 140 mm specimens at $R = -1$. As should be expected, smaller specimens show a higher fatigue strength than larger specimens. Run out specimens are specified with an arrow. The test data have been tabulated in Appendix A, Tables A1 and A2.

It should be noticed that one of the 120 mm \times 140 mm specimens was run out at stress amplitude of 130 MPa at 22 million cycles of fatigue life. This specimen was again tested at stress amplitude of 170 MPa and was broken. This specimen was specified with “Repeated” in Appendix A, Table A2. This specimen appears twice in Fig. 10, as a run out specimen at stress amplitude of 130 MPa and as a broken specimen at stress amplitude of 170 MPa.

3. Statistical analysis of fatigue data

If a large number of identical test pieces are run until fatigue failure, the number of cycles sustained will differ from specimen to specimen. The probability of failure, P , has to be introduced

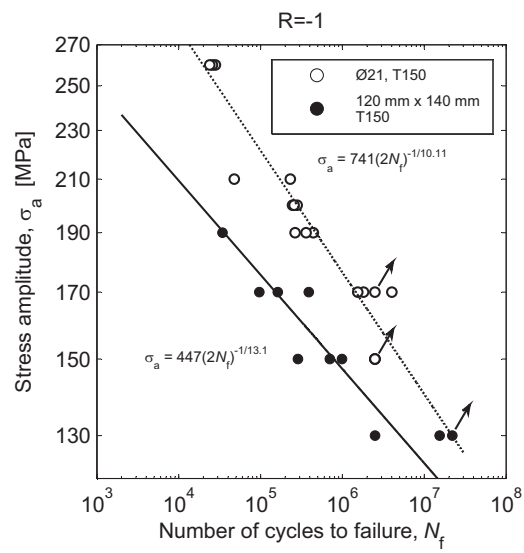


Figure 10: Fatigue behavior of EN-GJS-400-18-LT specimens with different dimensions cut from castings with 150 mm thickness.

and connected with the applied stress, σ , and the number of cycles to failure, N . These three parameters can be expressed in a $P - S - N$ diagram. This contains a family of $S - N$ curves, each curve corresponding to a particular value of the probability of failure, P .

The main purpose of this research is to present the obtained test results on fatigue behavior of heavy section EN-GJS-400-18-LT cast iron components and evaluation of geometrical size effect, technological size effect and saturation in geometrical size effect. In order to do this, a short overview of the required statistical analysis is presented in this research. Detailed explanation on statistical methods used in this research is given in Ref. [7].

3.1. Average $S - N$ curve

The $S - N$ curve is often assumed to follow the Basquin equation

$$\sigma_a = \sigma'_f (2N_f)^{-\frac{1}{m}} \quad , \quad (1)$$

where σ'_f is the fatigue strength coefficient and $-1/m$ the fatigue strength exponent. This curve will be a straight line on a log-log plot and may be found by linear regression analysis of fatigue data points. The average $S - N$ curves obtained by linear regression analysis of $S - N$ data with stress amplitude as the independent variable are presented in Fig. 10.

3.2. Weibull fatigue strength distribution

The first step to establish $P - S - N$ diagram for the tested specimens, is to model their fatigue strength or life distribution. The two-parameter Weibull distribution was used to model the fatigue strength of the specimens tested in this research. A weakest-link analysis can be formulated in two different ways, volume formulation and surface formulation [12]. In the volume formulation, the critical flaw is assumed to lie somewhere within the volume of the specimen. In the surface formulation, the controlling defects are assumed to be located at the surface of the specimen.

According to Weibull's weakest-link theory [12], the probability of component failure P , can be expressed as

$$P_f = 1 - \exp \left[- \left(\frac{\bar{\sigma}_a}{\sigma_{A0}^*(N)} \right)^{b_\sigma} \right] \quad . \quad (2)$$

where b_σ and $\sigma_{A0}^*(N)$ are shape and scale parameters, respectively.

The Weibull stress amplitude $\bar{\sigma}_a$, which may also be referred to as the fatigue-effective stress amplitude, for volume formulation is defined as

$$\bar{\sigma}_a = \left(\frac{1}{V_0} \int_V \sigma_a^{b_\sigma} dV \right)^{\frac{1}{b_\sigma}} \quad . \quad (3)$$

where V is the component volume. V_0 is an arbitrary reference volume, which may be thought of as the gage volume of the smooth fatigue specimens used to determine the $P - S - N$ data of the material. The Weibull shape parameter b_σ , is a measure of the scatter of the fatigue strength

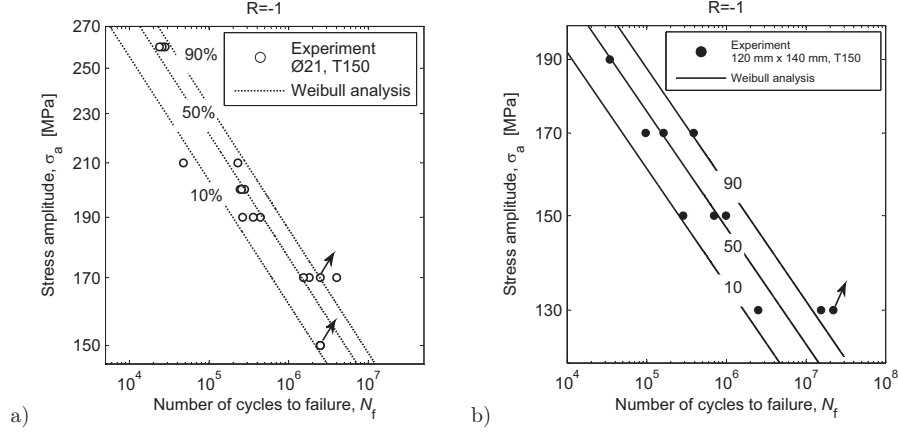


Figure 11: $P - S - N$ diagrams for (a) $\varnothing 21$ specimens, (b) $120 \text{ mm} \times 140 \text{ mm}$ specimens.

and, indirectly, a measure of the scatter of the defect size distribution. b_σ increases with decreasing scatter in the fatigue strength.

The Weibull stress amplitude $\bar{\sigma}_a$ or the fatigue-effective stress amplitude, for surface formulation is now defined as

$$\bar{\sigma}_a = \left(\frac{1}{A_0} \int_A \sigma_a^{b_\sigma} dA \right)^{\frac{1}{b_\sigma}} . \quad (4)$$

where A is the component surface area. A_0 is an arbitrary reference surface area, which may be thought of as the gage surface area of the smooth fatigue specimens used to determine the $P-S-N$ data of the material.

3.3. $P - S - N$ diagram

Once the fatigue life distribution is known, it will be possible to establish the $P-S-N$ diagram. To perform the statistical analysis, Minitab [19] was used and Weibull distribution parameters were obtained by least squares method. By fitting the Weibull distribution to the fatigue data points, $b_\sigma = 22.37$ was obtained for $\varnothing 21$ specimens and $b_\sigma = 20.34$ for $120 \text{ mm} \times 140 \text{ mm}$ specimens.

Figures 11a and 11b show the established $P-S-N$ diagrams for $\varnothing 21$ and $120 \text{ mm} \times 140 \text{ mm}$ specimens. The $S-N$ curves for probabilities of failure of 10, 50 and 90 percent shown in Fig. 11 are in good agreement with the distribution of data points.

The reader is referred to Ref. [6] for detailed explanation of the methodology used to find Weibull distribution parameters and establish the $P-S-N$ diagrams.

4. Geometrical size effect

The current design of large wind turbine cast components is based on safe life design philosophy. In the safe life design, $S - N$ curves are derived from fatigue testing on baseline material. To implement these $S - N$ curves in design of a real component, several reduction factors must be used to account for different parameters, one of them is geometrical size effect. In order to obtain the reduction factor corresponding to geometrical size effect, Weibull's weakest-link method may be used.

To evaluate the geometrical size effect, the small $\varnothing 21$ and large heavy section $120 \text{ mm} \times 140 \text{ mm}$ specimens were tested in this research. The specimens were from the cast blocks with 150 mm thickness. By using equations (2) and (3) or (4), it will be possible to predict the fatigue strength of larger $120 \text{ mm} \times 140 \text{ mm}$ specimens based on $\varnothing 21$ specimens $P - S - N$ diagram. According to Weibull's weakest-link theory, for a given material, life and probability of failure, the fatigue-effective stress amplitudes due to equations (3) or (4) should be the same for components with different dimensions, if there is no any saturation in size effect. Thus for components designated 1 and 2

$$\left(\int_{V_1} \sigma_{a1}^{b_\sigma} dV \right) = \left(\int_{V_2} \sigma_{a2}^{b_\sigma} dV \right) , \quad (5)$$

$$\left(\int_{A_1} \sigma_{a1}^{b_\sigma} dA \right) = \left(\int_{A_2} \sigma_{a2}^{b_\sigma} dA \right) . \quad (6)$$

Both equations (5) and (6) can be used to evaluate the effect of size on fatigue strength. Eq. (5) assumes the critical flaw to lie somewhere within the volume of the specimen (volume formulation) and Eq. (6) assumes the critical flaw to lie on the surface of the specimen (surface formulation). Using equations (5) or (6), it will be possible to estimate the $P - S - N$ diagram for $120 \text{ mm} \times 140 \text{ mm}$ specimens, based on the $P - S - N$ diagram of $\varnothing 21$ specimens shown in Fig. 11a. In order to calculate equations (5) and (6) over the components, an in-house finite element post-processor, P•FAT, was used. P•FAT is designed as a finite-element post-processor with the component geometry and stresses given by a standard finite element program. The reader is referred to Refs. [12, 20] for the theoretical and numerical aspects of the P•FAT weakest link module.

Fig. 12 shows the comparison of the estimated $120 \text{ mm} \times 140 \text{ mm}$ $P - S - N$ diagram obtained by equations (5) and (6) with experimental data. Both equations yield nearly the same results. The dashed lines show the estimated $120 \text{ mm} \times 140 \text{ mm}$ $P - S - N$ diagram based on $\varnothing 21$ $P - S - N$ diagram, the full lines show the $P - S - N$ diagram obtained by Weibull analysis of the original $120 \text{ mm} \times 140 \text{ mm}$ $S - N$ data. As noticed above, both volume and surface formulation of weakest link method gave the same estimation for $120 \text{ mm} \times 140 \text{ mm}$ $P - S - N$ diagram. Table 3 compares the size factors, σ_{a2}/σ_{a1} , predicted by equations (5) and (6) based on $\varnothing 21$ specimens.

As Fig. 12 shows, the estimated $S - N$ curves for $120 \text{ mm} \times 140 \text{ mm}$ specimens based on $\varnothing 21$ specimens test data, are close to the experimentally established $S - N$ curves (Weibull analysis) at low lives, but deviate from them by increasing the fatigue life. This is due to different slopes of $S - N$ curves for $\varnothing 21$ and $120 \text{ mm} \times 140 \text{ mm}$ specimens.

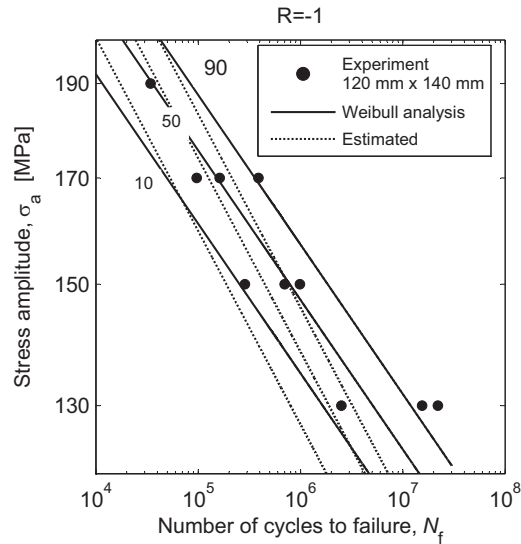


Figure 12: Comparison of estimated $P-S-N$ diagram for $120 \text{ mm} \times 140 \text{ mm}$ specimens obtained by weakest-link analysis with experimental data.

According to weakest-link theory, $S-N$ curves for $\varnothing 21$ and $120 \text{ mm} \times 140 \text{ mm}$ specimen should be parallel, but as Fig. 10 shows, the slope of the $S-N$ curve for $\varnothing 21$ specimens is different from the slope of the $S-N$ curve for $120 \text{ mm} \times 140 \text{ mm}$ heavy section specimens. $\varnothing 21$ specimens were tested up to 4 million cycles of fatigue life and the lowest stress amplitude which was used to test them is 150 MPa. But the heavy section specimens were tested up to 22 million cycles and the lowest stress amplitude which was used to test them is 130 MPa. The very long lives obtained for $120 \text{ mm} \times 140 \text{ mm}$ heavy section specimens at stress amplitude of 130 MPa change the slope of $S-N$ curve for these $120 \text{ mm} \times 140 \text{ mm}$ specimens relative to $\varnothing 21$ specimens. In fact, if the fatigue test results at stress amplitude of 130 MPa for $120 \text{ mm} \times 140 \text{ mm}$ heavy section specimens are not considered in the curve fitting calculations, the slope of $S-N$ curve for these heavy section specimens changes from $-1/13.1$ to $-1/11.2$ which is close to the slope of $S-N$ curve for $\varnothing 21$ specimens.

4.1. Saturation in geometrical size effect

As noticed above, by increasing component size, the fatigue strength decreases. Kaufmann [8] has performed fatigue tests on GJS-400 specimens and reported saturation in size effect at a gage volume of $8\,000 \text{ mm}^3$, but Shirani and Härkegård [6] has performed axial fatigue tests on

Table 3: Comparison of the size factors predicted by volume and surface formulation of weakest-link method based on $\varnothing 21$ specimens results.

Size factor	$\frac{\sigma_{a120 \times 140}}{\sigma_{a\varnothing 21}}$
Volume formulation	0.785
Surface formulation	0.771

EN-GJS-400-18-LT specimens with 21 and 50 mm diameter and did not observe any saturation in size effect up to a gage volume of 350 000 mm³. According to Ref. [6], the volume formulation of Weibull's weakest-link method yields a satisfactory estimation of the $P - S - N$ diagram for larger EN-GJS-400-18-LT specimens based on the $P - S - N$ diagram of smaller specimens.

In this research, the volume of the material subjected to 90% of the peak value of maximum principal stress in axial fatigue testing in 120 mm \times 140 mm heavy section specimens, Fig. 5b, is around 6 400 000 mm³. As Fig. 12 shows, the volume formulation of Weibull's weakest-link method predicts the size effect well up to to the largest investigated EN-GJS-400-18-LT specimens and the comparison of estimated $P - S - N$ diagram for 120 mm \times 140 mm specimens with experimental results does not show saturation in geometrical size effect.

5. Technological size effect

As noticed above, the morphology of the graphite in cast iron significantly influences the mechanical properties. By increasing the casting thickness, the cooling rate decreases and the fatigue strength decreases. In ductile cast iron, by decreasing the cooling rate, the nodularity and nodule count of the microstructure decreases [13-16].

The $\varnothing 21$ specimens tested in this research were from the cast blocks with 150 mm thickness, T150. The fatigue test results for $\varnothing 21$ specimens from initial blocks with 95 mm thickness, T95, are presented in Ref. [6]. To evaluate the casting thickness effect on fatigue strength, the fatigue test results for $\varnothing 21$ specimens from T95 blocks were compared with the fatigue test results for $\varnothing 21$ specimens from T150 blocks. Fig. 13 shows this comparison. As Fig. 13 shows, fatigue specimens from blocks with 95 mm thickness, show better fatigue strength comparing to the same specimens but from blocks with 150 mm thickness. As noticed above, this difference in fatigue strength is due to different microstructure of the specimens.

To evaluate microstructural effect on fatigue strength, metallography analysis was performed on 12 broken fatigue specimens, 6 specimens from T95 blocks and 6 specimens from T150 blocks. Detailed explanation on metallography analysis is given in Appendix B.

Table 4 shows the comparison of average microstructural properties of analyzed specimens from T95 and T150 material.

As Table 4 shows, both T95 and T150 material has the same nodularity, but T150 material has lower nodule count and subsequently larger graphite nodules. This difference in graphite nodule size explains the difference between fatigue strength of T150 and T95 material. The difference

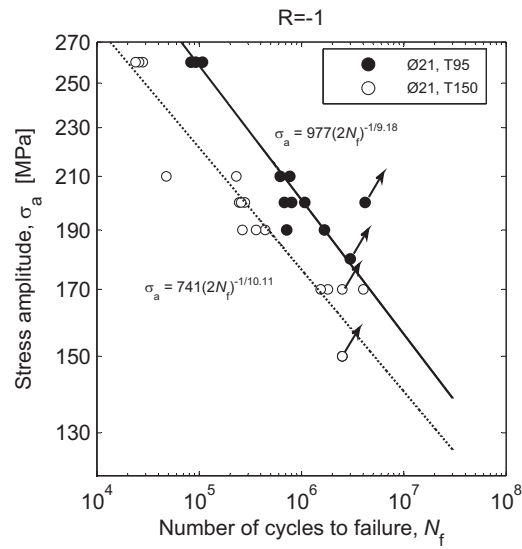


Figure 13: Comparison of fatigue test results for $\varnothing 21$ specimens from T150 blocks with the fatigue test results for the same $\varnothing 21$ specimens but from T95 blocks [6].

Table 4: Comparison of average microstructural properties, T95 vs. T150.

Material	Quantity	Nodularity (%)	Nodule count (mm^{-2})	Mean nodule diameter (μm)	Graphite content ¹ (%)	Pearlite content ² (%)
T150	Average	95.7	41.7	57.8	12.5	15.4
T95	Average	94.1	94	38.3	11.3	6.17
T150	Standard deviation	3.44	9.17	8.1	0.5	4.67
T95	Standard deviation	3.94	28.4	5.47	0.47	2.41

¹Percentage of total measured area.

²Percentage of total matrix area.

between nodule count and graphite nodule size in T95 and T150 material is clearly shown in Fig. 1. Both Figures 1 a and b show the area of the microstructure with the same size, but Fig. 1a, T150, contains fewer graphite nodules than Fig. 1b.

In fact, in baseline ductile cast iron, which does not contain major defects, graphite nodules work as shrinkage cavities. In fatigue crack initiation stage, micro-cracks initiate around these graphite nodules and then form the macro-crack which then propagates and leads to the final failure of the specimen. Thus, the T150 material which contains larger graphite nodules, contains larger micro-shrinkage cavities than T95 material and therefore needs a smaller number of cycles for a crack to initiate and propagate to become a macro-crack. This may explain the difference between the fatigue strength of the materials presented in Fig. 13.

6. Conclusions

Axial fatigue testing of EN-GJS-400-18-LT 120 mm \times 140 mm cross section specimens and \varnothing 21 cylindrical specimens was performed at room temperature at load ratio $R = -1$. The dimensions of the heavy section specimens are representative of large wind turbine castings. All specimens were machined from cast blocks with 150 mm thickness. Testing load levels for heavy section specimens were adjusted to yield fatigue lives from 10 000 to 14 million cycles, which is the typical range of endurance for wind turbine ductile cast iron components. Statistical analysis of fatigue test results was performed and Weibull distribution was used to model fatigue strength distribution. $P - S - N$ diagrams were established for tested specimens. To evaluate the geometrical size effect, weakest link method was used to predict $P - S - N$ diagram for 120 mm \times 140 mm specimens based on the $P - S - N$ diagram of \varnothing 21 specimens. The predicted $P - S - N$ diagram was compared with the experimentally established $P - S - N$ diagram for 120 mm \times 140 mm specimens. To evaluate the wall thickness effect on fatigue strength of this material, the obtained test results for \varnothing 21 specimens from initial blocks with 150 mm thickness were compared with the published test results on fatigue strength of the same \varnothing 21 specimens but from the cast blocks with 95 mm thickness. Metallography of both T95 and T150 material was performed, important microstructural parameters were measured and compared. Finally the effect of casting thickness on microstructure and the effect of microstructure on fatigue strength of this material was evaluated.

Acknowledgments

The authors would like to acknowledge financial and technical support by FeVIND, a project under the auspices of the Research Council of Norway. In particular, thanks are due to Vestas Wind Systems AS for providing the cast material and supporting the fatigue testing. The fatigue tests were carried out to our full satisfaction by Dr. P. Kucharczyk, IEHK, RWTH, Aachen. The authors also would like to thank Bente Thomsen, Material Laboratory, Vestas Technology R&D, for her careful metallography analysis.

Appendix A. $\varnothing 21$ and $120 \text{ mm} \times 140 \text{ mm}$ specimens fatigue test data

Table A1. $\varnothing 21$ specimen fatigue test data, Load Ratio $R=-1$.

Specimen number	Stress amplitude (MPa)	Fatigue life	Comment
1	150	2 500 000	Run out
2	150	2 500 000	Run out
3	150	2 500 000	Run out
4	170	1 537 919	Broken
5	170	1 814 046	Broken
6	170	2 500 000	Run out
7	170	4 017 251	Broken
8	190	264 153	Broken
9	190	359539	Broken
10	190	441 293	Broken
11	200	245 862	Broken
12	200	256 700	Broken
13	200	279 605	Broken
14	210	47 708	Broken
15	210	230 695	Broken
16	260	23 877	Broken
17	260	25 832	Broken
18	260	28 106	Broken

Table A2. $120 \text{ mm} \times 140 \text{ mm}$ specimen fatigue test data, Load Ratio $R=-1$.

Specimen number	Stress amplitude (MPa)	Fatigue life	Comment
1	130	2 509 326	Broken
2	130	15 442 945	Broken
3	130	22 000 000	Run out
4	150	285 846	Broken
5	150	701 057	Broken
6	150	987 192	Broken
7	170	96 664	Broken
8	170	162 404	Broken
3, Repeated	170	388 073	Broken
9	190	34 225	Broken

Appendix B. Metallography analysis

Metallography analysis was performed using Image-Pro Analyzer software [21]. For each specimen, measurements were performed on an area of 32 mm^2 close to the fatigue crack initiation site. The graphites were classified by their forms and sizes according to ISO 945-1 [22].

A possible classification of the different graphite forms as a function of sphericity and aspect ratio is shown in Fig. B1. The sphericity of a graphite is defined as the squared ratio of the perimeter of

a circle with the same area as the given graphite particle to the perimeter of the graphite particle, 1 for a perfect circle and close to 0 for very tortuous shapes. The aspect ratio of a graphite particle is defined as the ratio of minor axis to major axis length of an ellipse encapsulating the graphite nodule.

There is no unique mathematical definition for different graphite forms. The definition shown in Fig. B1 has been suggested by the authors and based on the evaluation of the different reference images given in ISO 945-1 [22] for different graphite forms.

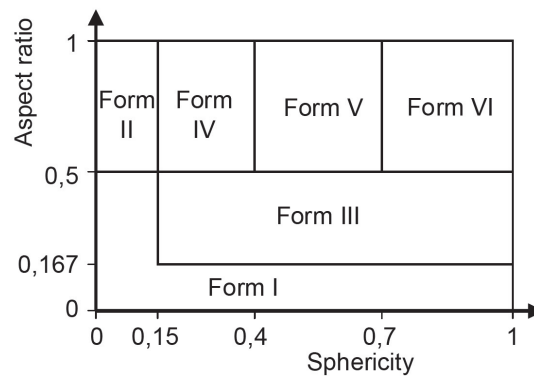


Fig. B1. Definition of the different graphite forms.

Table B1 shows the comparison of classified graphite forms average as percentage of total graphite area for the evaluated specimens from T95 and T150 material.

Table B1. Comparison of classified graphite forms average, T95 vs. T150.

Classified graphite form	Percentage of total graphite area T95 material	Percentage of total graphite area T150 material	Standard deviation T95 material	Standard deviation T150 material
IV	6	4.3	4	3.4
V	34	35	21	23.7
VI	60	60	24	27.1

As Table B1 shows, both T95 and T150 material contains almost the same amount of the graphite forms.

The size of the graphite nodules was also classified based on ISO 945-1 [22]. Table B2 shows the comparison of the classified graphite sizes average for the 12 analyzed T95 and T150 specimens.

Table B2. Comparison of classified graphite size average, T95 vs. T150.

Classified graphite size	Percentage of total graphite area T95 material	Percentage of total graphite area T150 material	Standard deviation T95 material	Standard deviation T150 material
4	0.5	10.4	1.13	9.3
5	26.5	63.1	14.7	11.3
6	58.3	24.5	9.6	15.8
7	14.1	1.6	6.91	0.75
8	0.57	0.4	0.30	0.46

As Table B2 shows, T95 material contains smaller graphite nodules than T150 material. This is due to the lower thickness and higher cooling rate of T95 material.

The fracture behavior of cast iron is influenced by nodularity and nodule size. For ductile cast iron with a given graphite content, larger graphite nodules lead to larger graphite nodule distance and lower nodule count. The nodularity or percentage of spheroidal graphite particles [23], is

$$Nodularity = \frac{\text{Area of acceptable graphite}}{\text{Total graphite area}} . \quad (7)$$

Highly spheroidal graphite has a considerably smaller stress concentrating effect than the graphite having vermicular, compacted or flake morphologies [24].

According to ISO 945-1 [22], graphite form V is the principal graphite form in thick walled castings made of spheroidal graphite cast iron. Therefore, to determine the nodularity in this research, both forms V and VI were accepted.

References

- [1] H. Roedter, M. Gagne, Ductile Iron for Heavy Section Wind Mill Castings: A European Experience, Proceedings of the 2003 Keith D. Millis World Symposium on Ductile Iron, South Carolina, 2003; paper 11.
- [2] Germanischer Lloyd, Guideline for the certification of offshore wind turbines, Edition 2005, Hamburg Germany.
- [3] Phillips C, Heywood R. The size effect in fatigue of plain and notched steel specimens loaded under reversed direct stress. *Proc Inst Mech Eng* 1951;165:113–24.
- [4] Gaenser H. Some notes on gradient, volumetric and weakest link concepts in fatigue. *Comput Mater Sci* 2008;44(2):230–9.
- [5] Carpinteri A, Spagnoli A, Vantadori S. Size effect in S–N curves: a fractal approach to finite-life fatigue strength. *Int J Fatigue* 2009;31(5):927–33.
- [6] M. Shirani, G. Härkegård, Fatigue life distribution and size effect in ductile cast iron for wind turbine components. *Eng Fail Anal* (2010), 18 (2011) 12–24.
- [7] EN 1563:1997, European standard, Founding – spheroidal graphite cast irons. CEN; June 1997.
- [8] Kaufmann H, Wolters D. Zyklische beanspruchbarkeit dickwandiger bauteile aus ferritischem guesen mit kugelgraphit. *Konstruieren Giessen* 2002;27(1):427.
- [9] Weibull W. A statistical theory of the strength of materials. *Ingeniörsvetenskapsakademiens handlingar*, vol. 151. Stockholm: Generalstabens Litograska Anstalts Förlag; 1939. p. 145.
- [10] Weibull W. The phenomenon of rupture in solids. *Ingeniörsvetenskapsakademiens handlingar*, vol. 153. Stockholm: Generalstabens Litograska Anstalts Förlag; 1939. p. 155
- [11] Weibull W. A statistical distribution function of wide applicability. *J Appl Mech* 1951;18(3):293–7.
- [12] Wormsen A, Sjödin B, Härkegård G, Fjeldstad A. Non-local stress approach for fatigue assessment based on weakest-link theory and statistics of extremes. *Fatigue Fract Eng Mater Struct* 2007;30(12):1214–27.
- [13] P. Emerson, W. Simmons, Final Report on the Evaluation of Graphite Form in Ferritic Ductile Irons by Ultrasonic and Sonic Testing and on the Effect of Graphite Form on Mechanical Properties, *AFS Trans* 84 (1976) 109-128.
- [14] G. Ru, B. Doshi, Relationship Between Mechanical Properties and Graphite Structure in Cast Irons. II. Ductile Iron, *Modern Casting* 70 (7) (1980) 70-74.
- [15] H. Itofuji, K. Kawamura, N. Hashimoto, H. Yamada, Production and Evaluation of Heavy-Section Ductile Cast Iron, *Transactions of the American Foundrymen’s Society*. 98 (1990) 585-595.
- [16] C. Loper Jr, Evaluation of Microstructural Factors Affecting Heavy-Section Ferritic DI Castings, in: *Ninety-Fifth Annual Meeting American Foundrymen’s Society*, 1991, pp. 543-549.

- [17] DIN 50125, Prüfung metallischer Werkstoffe—Zugproben, Normenausschuß Materialprüfung im Deutschen Institut für Normung. Berlin: Beuth-Verlag, 1991.
- [18] ASTM Standard E 466-07. Standard practice for conducting force controlled constant amplitude axial fatigue tests of metallic materials. West Conshohocken, PA (USA): ASTM International; 2007.
- [19] Minitab, release 15 for windows. State College (PA): Minitab Inc; 2007.
- [20] A. Wormsen, A. Fjeldstad, G. Härkegård, A post-processor for fatigue crack growth analysis based on a finite element stress field, *Computer Methods in Applied Mechanics and Engineering* 197 (6-8) (2008) 834-845.
- [21] Image-Pro® Analyzer, Version 6.3 for Windows, Media Cybernetics, Inc., Maryland
- [22] ISO 945-1: Designation of Microstructure of Cast Irons. Part 1. Graphite Classification by Visual Analysis (ISO 945-1:2008), European Committee for Standardization.
- [23] ASTM A247-67, Standard test method for evaluating the microstructure of graphite in iron castings, In: *Annual Book of ASTM Standards*, Vol. 01, 02, Am. Soc. Testing Mater., Philadelphia, 1998.
- [24] C.M. Ecob, A Review of Common Metallurgical Defects in Ductile Cast Iron. 9th Asian Foundry Congress, Hanoi, Vietnam, October 15–18, 2005.

Paper 3

Is not included due to copyright

Paper 4

Is not included due to copyright

Paper 5

Is not included due to copyright

Paper 6



Available online at www.sciencedirect.com



**Procedia
Engineering**

Procedia Engineering 2 (2010) 1125–1130

www.elsevier.com/locate/procedia

Fatigue 2010

Fatigue life prediction of components made of spheroidal graphite cast iron

M. Shirani^{a,*}, G. Härkegård^a, N. Morin^b

^aNorwegian University of Science and Technology, Dept. of Engineering Design and Materials, NO-7491 Trondheim, Norway

^bINSA de Lyon, Département Génie Mécanique et Développement, FR-69100 Villeurbanne, France

Received 26 February 2010; revised 10 March 2010; accepted 15 March 2010

Abstract

In many cast metals fatigue crack initiates from a defect. The lower bound of the fatigue life in cast components can be estimated based on the maximum defect size which is present in a component. In this research the distribution of defects in a ferritic spheroidal graphite cast iron component was determined. Then, Gumbel distribution was used to estimate the maximum sizes of defects in cylindrical fatigue specimens with different dimensions. Based on estimated maximum defect size, the fracture mechanics approach was used to determine the lower bound of the fatigue life for fatigue specimens with different dimensions and the geometrical size effect was modeled. © 2010 Published by Elsevier Ltd.

Keywords: Fatigue life prediction, Ferritic spheroidal graphite cast iron, Defects, Gumbel distribution

1. Introduction

In cast materials, the fatigue life is often controlled by the growth of cracks initiated from inclusions, nodules or other metallurgical defects [1-3]. Therefore to calculate the fatigue life or strength, such defect features can be considered as input parameters in fatigue life assessment. The effect of inclusions on fatigue strength can be studied by considering the defects as small cracks and use of the fracture mechanics [4-5].

Fatigue evaluation approaches for defect containing materials usually neglect the crack initiation stage [6-7]. Therefore fatigue life and fatigue limit are assumed to be controlled by the crack propagation law and by the threshold stress intensity factor, respectively. In a given volume of material subjected to the same cyclic stress, the fatigue crack initiates from the largest defect or inhomogeneity that is present in the volume. Thus, by estimating the size of maximum inclusion (or defect) which could be the origin of a prospective fatigue failure, it will be possible to predict the lower bounds of fatigue strength or fatigue life. Also, by estimating the maximum size of defects in specimens with different dimensions, it will be possible to model the geometrical size effect [8].

This size estimation can be done by using the statistics of extremes [9-10]. Defects data can be obtained with 'block maxima' or 'peak over threshold' sampling [11]. It was demonstrated by Murakami and co-workers that the

* Corresponding author. Tel.: +47-735-93761; fax: +47-735-94129.
E-mail address: mehdi.shirani@ntnu.no.

defects data obtained with such procedures ‘block maxima’ or ‘peak over threshold’, can be successfully described using the Gumbel distribution in order to calculate the dimension of the maximum occurring defect [12].

One possible approach to obtain the fatigue life as a function of the defect is to considering defects equivalent to pre-existent cracks. One typical method of expressing defect (or crack) size is the $\sqrt{\text{area}}$ parameter model in which the square root of the projected defect area is used as a representative parameter for defect size.

The main aim of this study is to predict the fatigue life for specimens made of ferritic spheroidal graphite cast iron and to model the geometrical size effect. $\sqrt{\text{area}}$ parameter model is used to obtain the fatigue life based on maximum defect size. Defect distribution within a ferritic spheroidal graphite cast iron component was determined using the ‘block maxima’ sampling. Then, Gumbel distribution was used to estimate the size of the largest defect in cylindrical fatigue specimens with different dimensions, Fig. 1. Finally a newly developed finite element post-processor, P•FAT, is used to determine the lower bound of the fatigue life of the specimens based on the largest estimated defect size. The lower bound of $S-N$ curves for fatigue specimens with different dimensions was obtained and the geometrical size effect was modeled.

2. Material and specimens

The material under investigation was EN-GJS-400-18-LT ductile cast iron with graphite nodules contained within a ferritic matrix. Table 1 summarizes the mechanical properties of the material [13]. Detail drawings of the specimens are shown in Fig. 1. Specimens were designed according to ASTM standard E 466 – 07 [14]. In order to evaluate the geometrical size effect two types of specimens with different volumes were used.

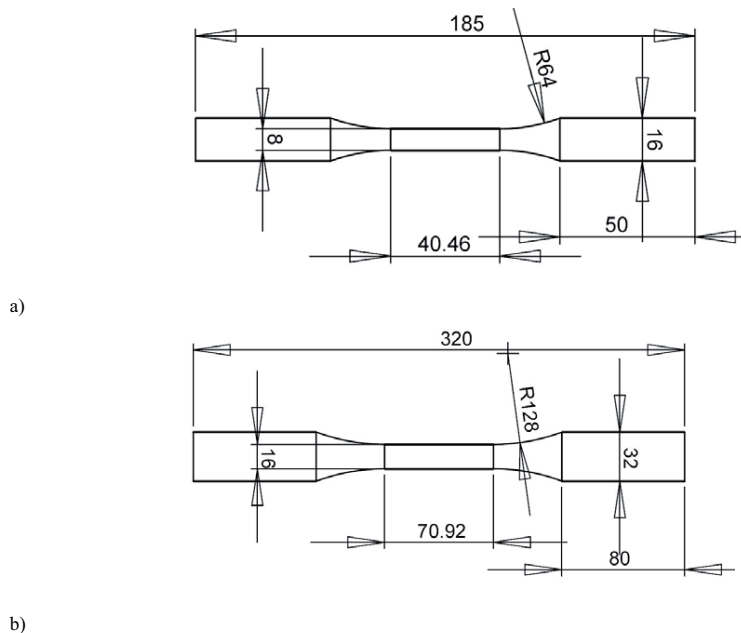


Fig. 1. Detail drawings of (a) Ø8 and (b) Ø16 specimens (all dimensions are in mm).

3. Inclusion rating

Gumbel distribution was used to estimate the size of the largest defect in cylindrical fatigue specimens shown in Fig. 1. The probability that the size X of the largest defect is less than a given size x can be expressed in terms of Gumbel's cumulative distribution function:

$$\Pr(X \leq x) = F(x) = \exp\left\{-\exp\left[-\frac{(x-\lambda)}{\delta}\right]\right\}, \quad (1)$$

where λ and δ are the location and scale parameter, respectively. From Eq. 1, the P -th percentile of the distribution is

$$x(P) = \lambda - \delta \cdot \ln(-\ln P). \quad (2)$$

If V is the volume of the component under examination and V_0 is the inspection volume for detecting the defects, the maximum defect occurring once in the component has a return period $T=V/V_0$ and cumulative probability $P = (1-1/T)$. By substituting the cumulative probability $P = (1-1/T)$ into Eq. 2, the dimension of defect in a component with V volume is:

$$x(T) = \lambda - \delta \cdot \ln\left[-\ln\left(1 - \frac{1}{T}\right)\right]. \quad (3)$$

The estimation of the distribution parameters fitting a given sample of defects can be done using different statistical methods.

There have been developed some methods to obtain 2D or 3D distribution of defects using 3D X-ray computed tomography [15] or optical inspection [16]. In this research optical inspection and the 'block maxima' sampling method was used to obtain the defect distribution in a ferritic spheroidal graphite cast iron. Several specimens were cut out of a cast iron component and the maximum area of defects in polished sections of these specimens was measured. All specimens had the same standard inspection area. Since \sqrt{area} parameter model is used to represent the defects size, the maximum defect area in each specimen was measured. Measurement of defects was done on $n = 56$ standard inspection surfaces with an area $S_0 = 150 \text{ mm}^2$. The area of the maximum defect in each standard area was measured by image analysis software. The obtained data are 2D, the exact value of $\sqrt{area_{max}}$ cannot be predicted with this 2D data. In order to estimate the exact amount of $\sqrt{area_{max}}$ in a volume, the obtained data should be 3D instead of 2D. The method proposed in Ref [5] was used to transform the inspection area S_0 to inspection volume V_0 by assigning a certain thickness to the 2D area S_0 . The mean value of the $\sqrt{area_{max}}$ previously measured is taken empirically as an appropriate value of the thickness h

$$h = \frac{\left(\sum \sqrt{area_{max,i}}\right)}{n}, \quad (4)$$

and the standard inspection volume is $V_0 = h \times S_0$.

By using the 'least squares' method to fit the Gumbel distribution to the square root of the measured maximum defect areas, λ and δ are obtained to be 0.106 mm and 0.0941 mm, respectively. The inspection volume for detecting the defects, V_0 , was obtained to be 20 mm^3 .

4. Size effect

As shown in the above section, by increasing the volume of the specimen, the maximum defect size will increase. In order to estimate the lower bound of fatigue strength or life for fatigue specimens shown in Fig. 1, with 2034 mm^3 and 14260 mm^3 gage volume, the maximum sizes of defects in these specimens are required. The return period for these specimens is 102 and 713, respectively. By using Eq. (3) the estimated maximum \sqrt{area} in these specimens will be 0.54 mm and 0.72 mm, respectively.

5. Fatigue life prediction

By having the maximum defect size in fatigue specimens, it will be possible to estimate the lower fatigue life bound for these specimens.

An in-house developed finite element post-processor, P•FAT, was used to perform the fatigue crack growth calculations. To obtain the fatigue life, defects are considered equivalent to pre-existent cracks. The crack like defects are assumed to grow on the plane of maximum principal stress. Failure of a component occurs if the stress intensity factor K has reached the fracture toughness K_{1C} . Paris-Erdogan law was used for fatigue crack growth calculations

$$da/dN=C(\Delta K)^m, \quad (5)$$

where da/dN is crack growth rate and ΔK is stress intensity range. C and m are crack growth constant and crack growth exponent, respectively. The values of C and m for the material used in this research are given in Table 1. The crack growth constants represented in Table 1 are for load ratio of $R = 0.1$. Walker equation was used to consider the mean load effect

$$\Delta K^* = \frac{\Delta K}{(1-R)^{1-\gamma}}, \quad R = \frac{K_{\min}}{K_{\max}}, \quad (6)$$

where γ is the walker exponent. The constant C of the crack growth law, the stress range, the fatigue limit and the threshold stress intensity range can all be transformed to $R = 0$ by using Walker's equation as shown in [17,18]. The exponent m of the crack growth law generally varies only weakly with R [19] and is assumed to be constant in this work. The value of γ for the material used in this research is given in Table 1.

Weight functions [20], together with the stress field of the crack free component, are used to compute the required stress intensity factors. To calculate the fatigue life, P•FAT needs stress distribution in the fatigue specimen. The fatigue specimen was modeled in ABAQUS. A reference axial load was applied to fatigue specimen and stress distribution over the component was determined. Fig. 2 shows stress distribution in Ø16 fatigue specimen. To perform fatigue crack growth calculation, FE model was imported in P•FAT. Defect was inserted on the surface of specimen, Fig. 3, and crack growth analysis was performed to develop the crack and calculate the fatigue life. In order to obtain $S-N$ curves, fatigue lives were obtained at different stress amplitudes. The obtained $S-N$ curves which represent the lower bound of fatigue life for Ø8 and Ø16 specimens are shown in Fig. 4. Table 1 shows material properties used in simulations.



Fig. 2. Stress distribution in Ø16 fatigue specimen.



Fig. 3. Defect inserted on the Ø16 fatigue specimen surface.

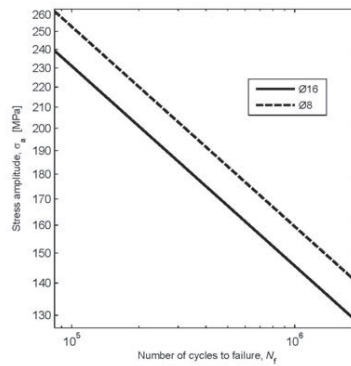


Fig. 4. The lower bound of *S-N* curve for Ø8 and Ø16 specimens

Table 1. Material properties used in the simulations

Modulus of elasticity, E (GPa)	167
Crack growth exponent, m	5
Crack growth constant C (MPa, m)	4.27×10^{-13}
Stress ratio for the crack growth constant, R	0.1
Walker exponent, γ	0.44

6. Conclusion

The defect distribution was obtained in a ferritic spheroidal graphite cast iron. Gumbel distribution was used to model the defect distribution. Maximum size of defects in fatigue specimens with different dimensions were estimated by Gumbel distribution. Fatigue crack growth simulations were performed to determine the lower bound of *S-N* curves for fatigue specimens. The lower bound of fatigue life for fatigue specimens was obtained based on the estimated maximum defect size. The geometrical size effect was modeled for fatigue specimens with different volumes.

Acknowledgements

The authors would like to acknowledge financial and technical support by FeVIND, a project under the auspices of the Research Council of Norway. In particular, thanks are due to Siemens Wind Power AS, Denmark for providing the cast material and supporting the metallographic investigations.

References

- [1] T. Palin-Luc, S. Lasserre, J. Berard, Experimental investigation on the significance of the conventional endurance limit of a spheroidal graphite cast iron, *Fatig Fract Eng Mater Struct* 2 (2) (1998) 191–200.
- [2] H. Agha, A. Beranger, R. Billardon, F. Hild, High-cycle fatigue behaviour of spheroidal graphite cast iron, *Fatig Fract Eng Mater Struct* 21 (3) (1998) 287–296.
- [3] Y. Nadot, J. Mendez, N. Ranganathan, A. Beranger, Fatigue life assessment of nodular cast iron containing casting defects, *Fatig Fract Eng Mater Struct* (UK) 22 (4) (1999) 289–300.
- [4] K. Miller, E. De los Rios, *The behaviour of short fatigue cracks*, Mechanical Engineering Publications, P. O. Box 24, Northgate Avenue, Bury St Edmunds, Suffolk IP 32 6 BW, UK, 1986.
- [5] Y. Murakami, *Metal fatigue: effects of small defects and nonmetallic inclusions*, Elsevier Science, 2002.
- [6] J. Ting, F. Lawrence, Modeling the long-life fatigue behavior of a cast aluminum alloy, *Fatig Fract Eng Mater Struct* (Print) 16 (6) (1993) 631–647.
- [7] B. Skallerud, T. Iveland, G. Härkegård, Fatigue life assessment of aluminum alloys with casting defects, *Eng Fract Mech* 44 (6) (1993) 857–874.
- [8] S. Beretta, A. Ghidini and F. Lombardo, Fracture mechanics and scale effects in the fatigue of railway axles, *Eng Fract Mech* 72 (2) (2005) 195–208.
- [9] E. Gumbel, *Statistics of extremes*, Dover Pubns, 2004.
- [10] S. Beretta, Y. Murakami, Statistical analysis of defects for fatigue strength prediction and quality control of materials, *Fatig Fract Eng Mater Struct* 21 (9) (1998) 1049–1066.
- [11] A. Fjeldstad, A. Wormsen, G. Härkegård, Simulation of fatigue crack growth in components with random defects, *Eng Fract Mech* 75 (5) (2008) 1184–1203.
- [12] Y. Murakami, H. Usuki, *Quantitative evaluation of effects of non-metallic inclusions on fatigue strength of high strength steels. II: Fatigue limit evaluation based on statistics for extreme values of inclusion size.*, *Int J Fatig* 11 (5) (1989) 299–307.
- [13] P. Hübner, H. Schlosser, G. Pusch, H. Biermann, Load history effects in ductile cast iron for wind turbine components, *Int J Fatigue* 29 (2007) 1788–1796.
- [14] Standard Practice for Conducting Force Controlled Constant Amplitude Axial Fatigue Tests of Metallic Materials, ASTM, 2004, p. E466.
- [15] M. Shirani, G. Härkegård, Fatigue Crack Growth Simulation in Components with Random Defects, *J. ASTM Int.* 6 (9) (2009)
- [16] K. Furumura, T. Abe, and Y. Murakami: in 'Bearing steels into the 21st century' (ed. J. J. C. Hoo and W. B. Green), STP 1327, 249–264, Philadelphia, PA, ASTM, 1998.
- [17] T. Mann, B.W. Tveiten, G. Härkegård, Fatigue crack growth analysis of welded aluminium RHS T-joints with manipulated residual stress level, *Fatigue Fract Engng Mater Struct* 29 (2) (2006) 113–22.
- [18] T. Mann, The influence of mean stress on fatigue crack propagation in aluminium alloys. *Int J Fatigue* 29 (8) (2007) 1393–1401
- [19] T. Mann, Fatigue assessments methods for welded structures and their application to an aluminium T-joint. PhD thesis, NTNU, Trondheim, Norway, 2006.
- [20] T. Fett, and D. Munz, Stress Intensity Factors and Weight Functions, *International Series on Advances in Fracture*, Computational Mechanics Publications, Southampton, 1997.

Paper 7

Is not included due to copyright

